Synthesis of *tripod* Ligands Containing Mixed Donor Sets with Phosphane and Pyrazole Donors – Bidentate Chelate Binding Modes and Dynamic Behaviour of *tripod* Ligands in d^8-Metal Complexes (Ni^{II}, Pd^{II}, Pt^{II})

Ralf Faissner,[a] Gottfried Huttner,*[a] Elisabeth Kaifer,[a] Peter Kircher,[a] Peter Rutsch,[a] and Laszlo Zsolnai[a][†]

Dedicated to Professor Rolf Gleiter[‡]

Keywords: Tripod ligands / Conformation / Nickel / Palladium / Platinum

The synthesis of a series of *tripod* ligands $MeOCH_2C(CH_2X)(CH_2Y)(CH_2Z)$ (X = PR_2; Y, Z = PR'_2 or pz; pz = 1-pyrazolyl) based on the 3,3-difunctionalized oxetane $O^a[CH_2]_2C^a(CH_2OMs)(CH_2Br)(O^a–C^a)$ as the starting material is described. With their mixed donor sets these ligands coordinate to d^8-metal ions in a bidentate binding mode. One of the three donors remains uncoordinated in each case. Coordination of phosphane donors is generally preferred over coordination of pyrazole donors. With bulky phosphanes such as $–CH_2PMes_2$, however, pyrazole may compete with PR_2, depending on the kind of the d^8 fragment. Dynamic exchange between coordinated and noncoordinated pyrazole donors is observed. Tetracoordinate complexes of the general type L_2MR_2 are formed (L_2 symbolizes the *tripod* ligand in its bidentate chelate binding mode with two donors functions coordinating and the third one serving as a dangling arm; M = Ni^{II}, Pd^{II}, Pt^{II}). With nickel(II) as the d^8 species, tetrahedral or square-planar coordination geometries ensue, depending on the kind of donor functions and on the kind of co-ligands R. With palladium(II) and platinum(II) as the d^8 centres, square-planar coordination is observed throughout. The size of the chelate cycles varies from six to eight depending on the number of pyrazole entities within the cycle. The conformations and the conformational flexibility characterizing the chelate cycles have been analysed by X-ray analyses and by variable-temperature NMR. The classes of conformations observed may be formally reduced to chair, half-chair and twist-boat conformations. Dynamic exchange between these conformations is observed. In one case, the same compound forms two different types of crystals that differ by the conformation adopted by their chelate cycles. All compounds have been fully characterized by standard analytical techniques including X-ray structure analysis of 14 chelate compounds.

Introduction

The synthesis of neopentane-based *tripod* ligands $RCH_2C(CH_2X)(CH_2Y)(CH_2Z)$ that contain up to three different donor functions X, Y, Z, is generally well developed for different kinds of donor functions.[1–5] The selective introduction of nitrogen donor functions is, however, in most cases limited to special kinds of nitrogen donors[5] as well as to specific reaction schemes[5]. Pyrazole is a nitrogen-donor group of more general applicability in *tripod* synthesis[5e,5f] that may be especially easily incorporated in *tripod* ligands $HOCH_2C(CH_2pz)(CH_2PR_2)(CH_2X)$ by a series of nucleophilic substitutions and ring-opening reactions starting from the functionalized oxetane $O^a[CH_2]_2C^a(CH_2Br)(CH_2OMs)(O^a–C^a)$.[5e]

The scope of this type of reaction sequence was tested by applying different phosphorus nucleophiles as well as different nitrogen nucleophiles. The coordination properties of these ligands versus the d^8-metal ions nickel(II), palladium(II), and platinum(II) were tested to elucidate the competition between different types of donor groups. In such coordination compounds the potential *tripod* ligands will act as bidentate ligands with the third potential donor function uncoordinated.[5b,5f,6] The dynamic exchange between coordinated and uncoordinated ligand functions in *tripod* compounds as well as the conformation of the chelate cycles are also reported here.

Results

Ligand Synthesis

The *tripod* ligands **3** and **4** were obtained from oxetane precursors **2**, which were themselves synthesized from the functionally substituted oxetane **1** by standard procedures

[a] Anorganisch-Chemisches Institut der Universität Heidelberg, Im Neuenheimer Feld 270, 69120 Heidelberg, Germany
Fax: (internat.) + 496221/545707
E-mail: g.huttner@indi.aci.uni-heidelberg.de
[†] Deceased.
[‡] As a late contribution to his 65th birthday.

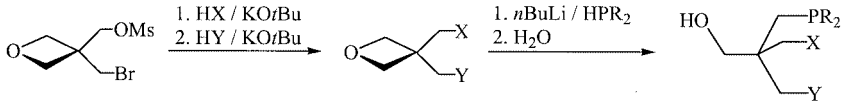

pz = 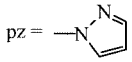

py = 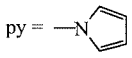

	X	Y
2a	PPh_2	pz
2b	PPh_2	py
2c	pz	pz

	PR_2	X	Y
3a	PPh_2	PPh_2	pz
3b	$P(m\text{-}Tol)_2$	PPh_2	pz
3c	$PMes_2$	PPh_2	pz
3d	PCy_2	PPh_2	pz
3e	PPh_2	PPh_2	py
4a	PPh_2	pz	pz
4b	$PMes_2$	pz	pz

Scheme 1. Synthesis of OH-functionalized *tripod* compounds

(Scheme 1).[5e] Some compounds (**2a**, **2c**, **3a**, **4a**) have already been described.[5e] All the compounds **2**–**4** were fully characterized by the usual spectroscopic techniques as well as by elemental analyses (see Exp. Sect. and Tables 10, 12, and 14).

The transformation of the *tripod* ligands **3** and **4**, which bear a CH_2OH group at the backbone, into the corresponding methyl ethers **5** and **6** followed the standard protocol (Scheme 2).[3i,7] None of the difficulties often observed in the etherification of analogous *tripod* ligands containing either three different P donors or P donors and Cp derived donor functions were encountered.[3i,4d,8] Analytical data of **5** and **6** are given in the Exp. Sect. and Tables 10, 12, and 14.

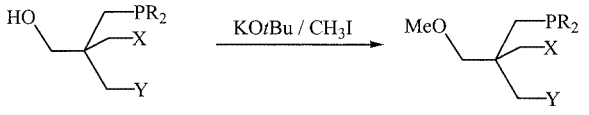

	PR_2	X	Y
5a	PPh_2	PPh_2	pz
5b	$P(m\text{-}Tol)_2$	PPh_2	pz
5c	$PMes_2$	PPh_2	pz
5d	PPh_2	PPh_2	py
6a	PPh_2	pz	pz
6b	$PMes_2$	pz	pz

Scheme 2. Synthesis of *tripod* ligands **5** and **6**

Coordination Chemistry

Coordination derivatives, in which compounds **5** and **6** bind to $MHal_2$ (M = Ni^{II}, Pd^{II}, Pt^{II}) as bidentate ligands, are obtained by standard procedures (see Exp. Sect.), in some cases as single crystals suitable for X-ray analysis (Scheme 3, Table 1).

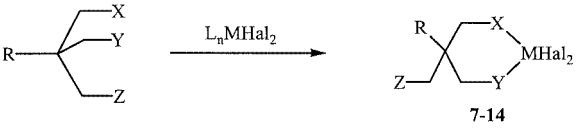

Scheme 3. Synthesis of coordination compounds **7**–**14**

Crystal structure analyses of metal complexes derived from the ligand **5a** were performed for compounds **7a**, **8**, and **9a** (Tables 2–4, 7, and Figures 1 and 2). All these compounds show a square-planar coordination around the metal centre. Ligand **5a** is observed to coordinate via its two PPh_2 donor groups exclusively while the pyrazole donor remains uncoordinated. The six-membered chelate cycle thus formed shows a half-chair conformation for **7a**, **8**, and **9a**. Figure 1 shows two examples. Within the chelate cycles showing a half-chair conformation (**7a/1**, **8**, **9a**) the CH_2OMe group occupies the axial position, with the more bulky CH_2pz group in the equatorial position throughout.

For **7a** two different crystal forms were obtained: one (**7a/1**·CH_2Cl_2) contains molecules with the chelate cycle in a half-chair conformation as well, and the other one (**7a/2**·$0.5CH_2Cl_2$) contains molecules in which the chelate cycle has a twist-boat conformation, showing that different conformations are accessible to the chelate cycles (Figure 2). These findings agree well with observations made on the chelate cycles in $[\{\kappa^2P\text{-}R_2PCH_2CH(OH)CH_2PR'_2\}Rh(\eta^4\text{-cod})]^+PF_6^-$. For this type of diphosphane-containing chelate cycle a thorough analysis of the conformation hypersurface[9] as well as of the NMR dynamics[7,10] revealed a small energy difference between half-chair and twist-boat conformations of the chelate cycle. This agrees well with the fact that **7a** forms two different types of ring conformation in its crystals under standard crystallization conditions.

Ligands containing one phosphane and two pyrazole N donors are found to coordinate to nickel(II) by one phosphorus and one nitrogen donor (**11a**, **11c**, see Table 1) or by two pyrazole donors with the CH_2PR_2 group playing the

Table 1. Coordination compounds **7–14**

Compd.	Ligand	Coord. groups X, Y		Noncoord. groups Z, R		$MHal_2$	Colour of compd.	Coord. geometry	Crystal structure
7a	**5a**	PPh_2	PPh_2	pz	CH_2OMe	$NiCl_2$	orange-coloured[a]	square-planar	yes
7b	**5b**	PPh_2	P(*m*-Tol)$_2$	pz	CH_2OMe	$NiCl_2$	orange-coloured	square-planar	no
7c	**5c**	PPh_2	$PMes_2$	pz	CH_2OMe	$NiCl_2$	ruby-coloured	square-planar	no
7d	**5d**	PPh_2	PPh_2	py	CH_2OMe	$NiCl_2$	orange-coloured	square-planar	no
8	**5a**	PPh_2	PPh_2	pz	CH_2OMe	$NiBr_2$	red	square-planar	yes
9a	**5a**	PPh_2	PPh_2	pz	CH_2OMe	$PdCl_2$	colourless	square-planar	yes
9b	**5b**	PPh_2	P(*m*-Tol)$_2$	pz	CH_2OMe	$PdCl_2$	pale yellow	square-planar	no
10	**5a**	PPh_2	PPh_2	pz	CH_2OMe	$PtCl_2$	colourless	square-planar	no
11a	**6a**	PPh_2	pz	pz	CH_2OMe	$NiBr_2$	violet	tetrahedral	yes
11b	**6a**	PPh_2	pz	pz	CH_2OMe	$NiCl_2$	violet	tetrahedral	no
11c	–[b]	PPh_2	pz	pz	CH_2OEt	$NiBr_2$	violet	tetrahedral	yes
12	**6a**	PPh_2	pz	pz	CH_2OMe	$PdCl_2$	yellow	square-planar	yes
13	**6b**	pz	pz	$PMes_2$	CH_2OMe	$NiCl_2$	blue–violet	tetrahedral	yes
14	–[c]	pz	pz	pz	Me	$NiBr_2$	blue	tetrahedral	yes

[a] In crystalline form: red. [b] Ligand $EtOCH_2C(CH_2PPh_2)(CH_2pz)_2$; synthesis see ref.[5e] [c] Ligand: $CH_3C(CH_2pz)_3$; synthesis see ref.[5e]

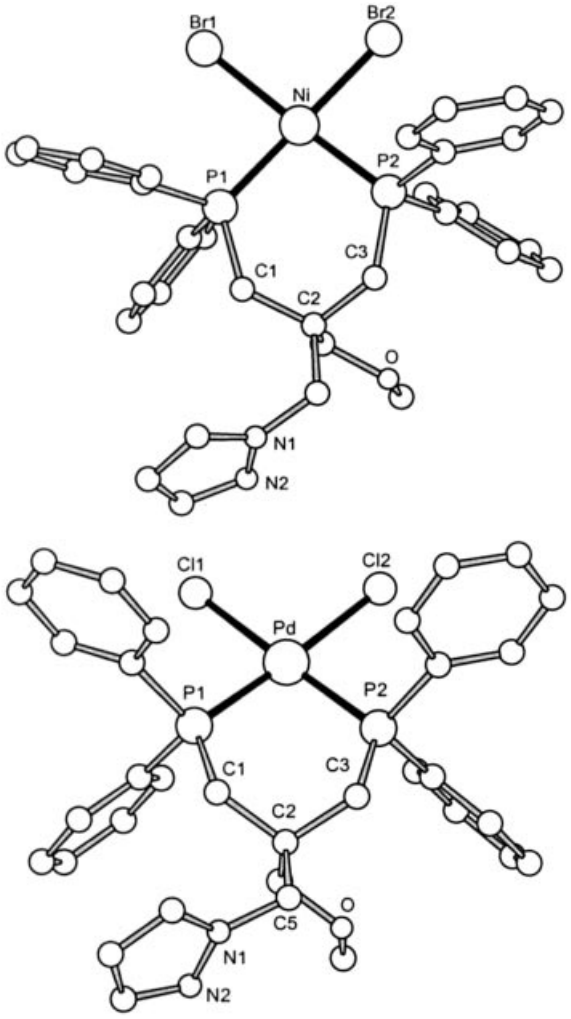

Figure 1. X-ray structure of compound **8** (top) and **9a** (bottom) derived from ligand **5a**

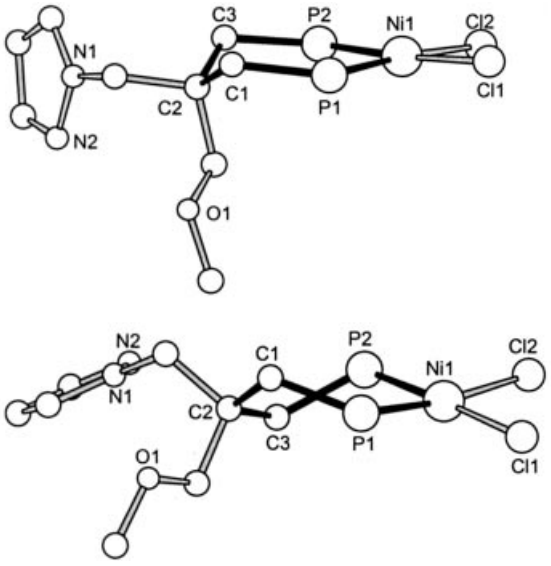

Figure 2. X-ray structure (without phenyl groups) of compound **7a/1** (top, half-chair conformation) and **7a/2** (bottom, twist-boat conformation)

role of a dangling arm (**13**, see Table 1). Figure 3 shows examples of the two coordination modes (*P*,*N* versus *N*,*N*). In addition to the ligands **6a** and **6b** two other *tripod* ligands containing a pz,pz donor set were used. Thus compounds **11c** and **14** (Table 1) are derived from ligands reported earlier.[5e] In each case the coordination geometry around nickel(II) is tetrahedral. Compounds **11a–c**, **13**, and **14** are paramagnetic – in contrast to compounds **7** and **8** with their square-planar nickel coordination.

Analytically pure **14** with its *tripod* ligand $CH_3C(CH_2pz)_3$[5e] crystallized as a conglomerate of different crystal forms, most of which were blue. Their structure corresponds to a tetrahedral coordination of the nickel atom as evidenced by crystallography (**14**, see Tables 1–4, 8). A few crystals were red-brown. Their quality was, however, insufficient for X-ray analysis. It is assumed that the difference in colour of these crystals is due to differing kinds of coordination, probably involving the formation of dinuclear entities with bromide acting as a bridging ligand. Thus, different chelate compounds containing $NiBr_2$ groups

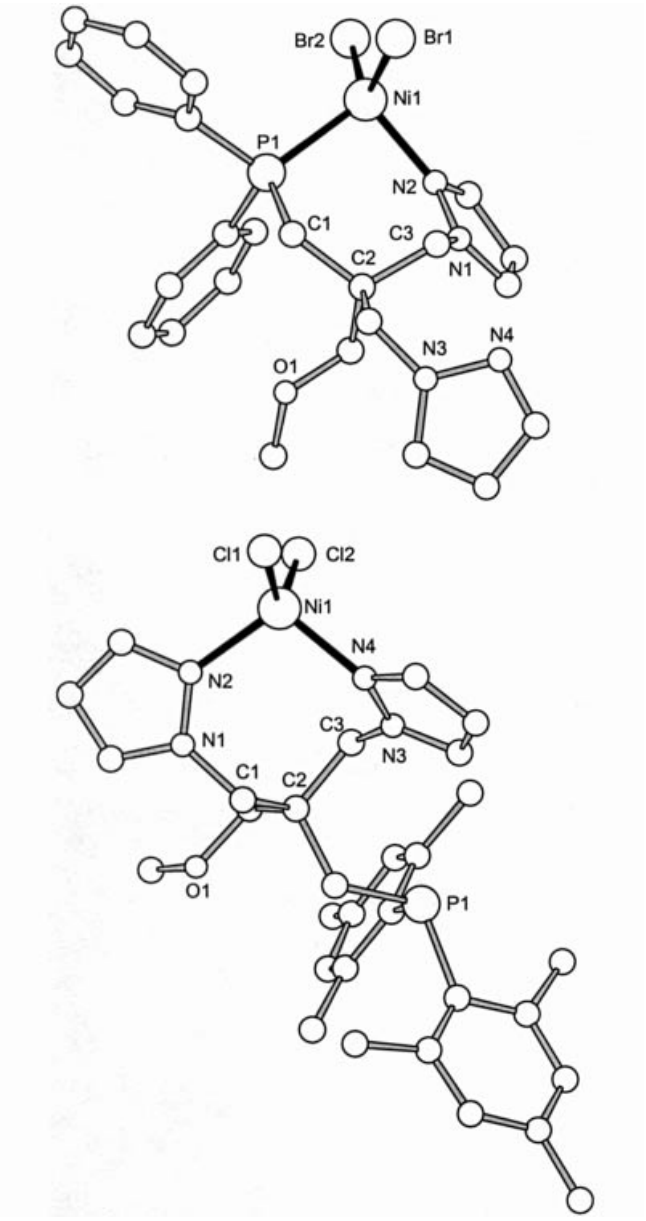

Figure 3. X-ray structure of compound **11a** (top) and **13** (bottom)

were prepared (**8**, **11a**, **11c**) in addition to **14**. The phenomenon could not be observed for **8** or **11a**. With **11c**, however, crystallization yielded violet crystals containing the tetrahedrally coordinated monomeric compound (analogous to **11a** depicted in Figure 3) and red-brown crystals containing the dinuclear species **15** (Figure 4). Both kinds of crystals were suitable for X-ray analysis. The nickel centres in **15** show idealized square-pyramidal coordination (τ = 0.16, see Figure 4).[11]

With palladium(II) as the central metal ligand **6a** acts as a P,N ligand resulting in **12** (Table 1). However, the coordination around the palladium(II) atom is square-planar (Figure 5), in contrast to the tetrahedral coordination of nickel(II) (**11**) by the same ligand arrangement.

With each pyrazole group replacing a one-atom donor group (e.g. PR_2) of a six-membered chelate cycle, the number of atoms within the cycle increases by one, such that *P*,*N*-coordinated compounds (**11**, **12**) have seven-membered chelate cycles and *N*,*N*-coordinated compounds (**13**, **14**) contain eight-membered chelate cycles. Because the pyrazole ligands are coplanar with their substituents − with the carbon atom bonded to one of its nitrogen centres and the metal atom coordinated to the other − the conformation of the chelate cycles may be characterized by an idealized graph with a pseudo corner (Q) at the centre of the pyrazole N−N bond (Scheme 4).

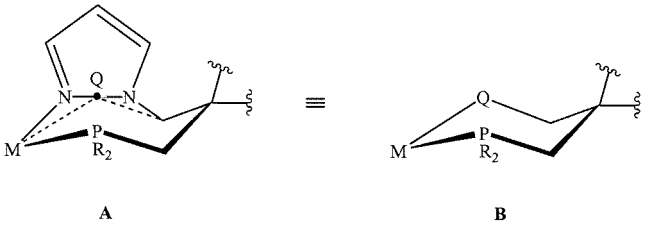

Scheme 4. Idealized graph for chelate cycles containing pyrazole donors: **A**: original; **B**: idealization

This kind of idealization reduces the pyrazole-containing chelate cycles to six-membered cycles (**B**, Scheme 4), even though they actually have seven or eight atoms within the cycle (**A**, Scheme 4) . The observed conformations may therefore be characterized in the same way as for six-membered cycles.

Table 2 indicates the conformation of the chelate cycles observed in each case. The difference between the two classes − (i) twist-boat and (ii) chair or half-chair − is most clearly evident from the pseudo torsion angle 3−2−6−5 (Table 2). Chair or half-chair conformations have 2−3 and 6−5 bonds that are almost parallel. The respective torsion angles are close to zero (deviation from −1.9 to +12.9°, see Table 2). For twist-boat conformations these bonds cannot be parallel, of course, and the corresponding torsion angles are between 44.3 and 67.0° (for absolute values, see Table 2). These two classes are, of course, also differentiated by the sequence of sign changes of the torsion angles around the cycles (columns M−2−3−4 to 6−M−2−3 in Table 2). The different types of conformation listed in Table 2 do obviously not reflect the either square-planar or tetrahedral coordination of the metal centre since the same types of conformations are found for both coordination modes.

Table 3 shows that the nickel−ligand distances respond significantly to the kind of coordination. Ni−P distances of ca. 217 pm are found for compounds showing a square-planar coordination of the nickel atom (Table 3) and of ca. 230 pm for tetrahedrally coordinated nickel compounds (Table 3). Ni−N distances have only been measured for compounds with tetrahedrally coordinated nickel atoms, and are 198 pm, within a few standard deviations, in each case (Table 3). As expected, all nickel compounds that contain at least one nitrogen donor in their chelate cycle show tetrahedral nickel coordination. The Ni−Cl and Ni−Br distances are around 221 and 236 pm, respectively (Table 3),

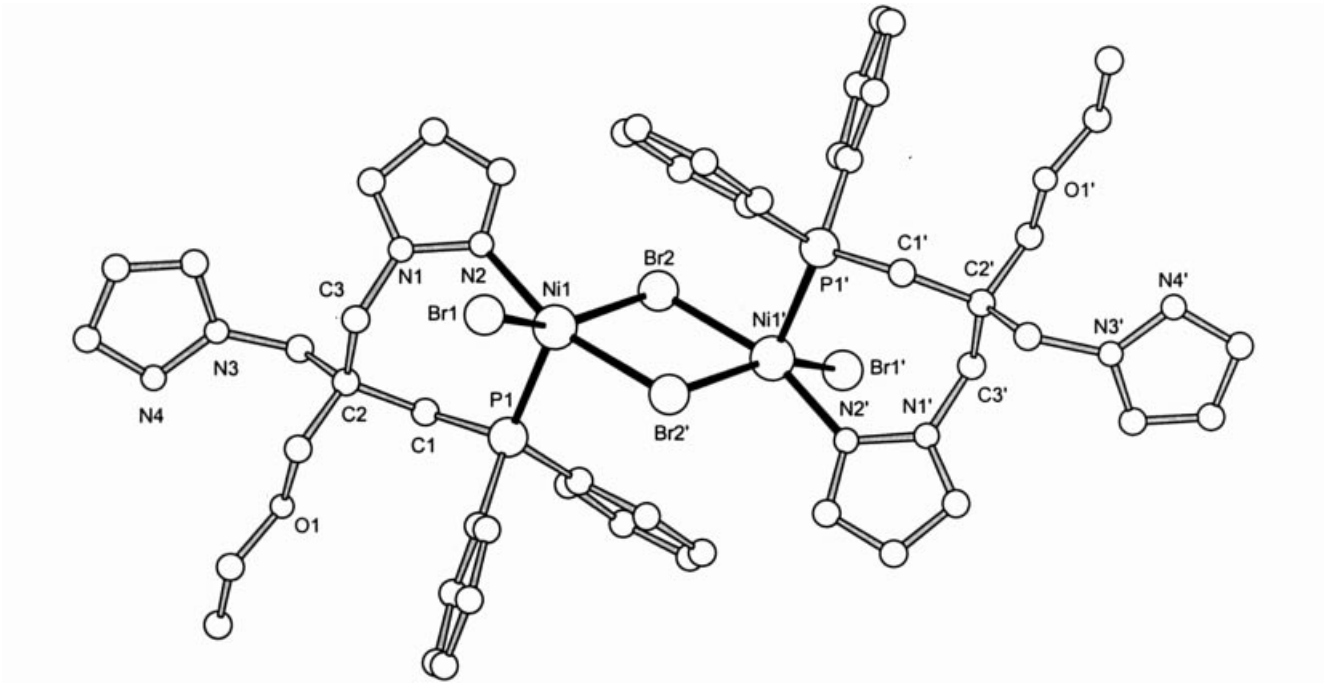

Figure 4. X-ray structure of the dinuclear nickel compound **15**; the compound is of crystallographic C_i symmetry

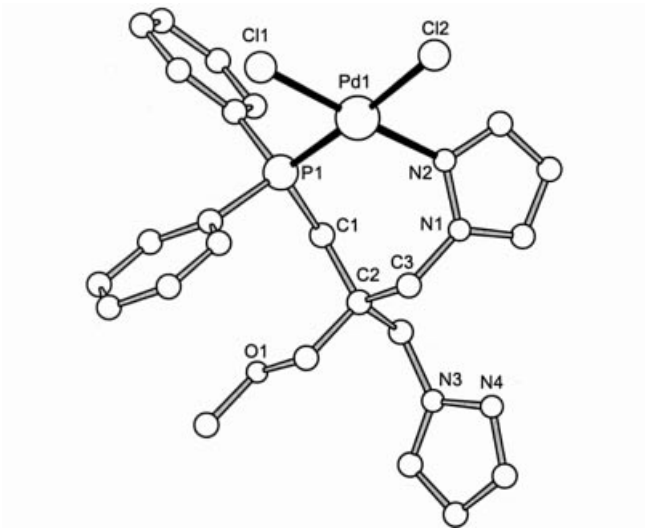

Figure 5. X-ray structure of compound **12**

with no detectable influence due to the kind of coordination geometry.

Compounds **9a** and **12** contain the palladium atom in a square-planar coordination with the chelate ligand coordinating via one N and one P donor (**12**). In **12** the Pd−Cl distances (Table 3) are influenced by their *trans* ligands, with the bond *trans* to the nitrogen donor [228.2(1) pm] being significantly shorter than that *trans* to the phosphorus donor [235.6(1) pm].

The Ni−P distance of the dinuclear compound **15** is 235.9 pm (Table 3, Figure 4), which is even longer than the Ni−P distances in compounds containing tetrahedrally coordinated nickel atoms. This corresponds to the apical position of the phosphorus donor in **15** (Figure 4). The Ni−Br distances are also longer than the Ni−Br distances observed in **8**, **11**, or **14** (Table 3). The shortest Ni−Br distance of **15** (245 pm) corresponds to the terminal Ni−Br bond. The bridging Ni−Br distances are still around 8 pm longer than this (Table 3). Consequently, all bonds are weakened by changing from tetra-coordination (**8**, **11**, and **14**) to penta-coordination (**15**). The fact that the monomeric arrangement in **11c** and the dimeric arrangement of the same compound in **15** are of almost equal energy is indicated by their co-crystallization as a conglomerate in the same experiment. The solubility of **11c** in CH_2Cl_2 is higher than that of **15**, such that attempts to dissolve red-brown **15** in CH_2Cl_2 led to violet solutions (Table 1) of **11c**.

The angles at the metal centre are in the ranges expected for square-planar and tetrahedral coordination (Table 4). In square-planar compounds the angles subtended by the coordinating atoms of the chelate ligands are somewhat larger than the ideal value of 90° (Table 4). For the tetrahedrally coordinated compounds these angles are smaller than expected for an ideal tetrahedron (109.4°, see Table 4). Deviation from this ideal value is greater for a P,N donor set (**11** and **12**, see Table 4) than for an N,N donor set (**13** and **14**, see Table 4).

NMR Dynamics

It is well known that L_2NiHal_2 (L = aryl phosphane) − even if square-planar in the solid state − may suffer distortions to tetrahedral arrangements at room temperature in solution such that no ^{31}P NMR signals are observed.[12]

When crystalline **7a**, which consists of crystals with the ligand in the chair conformation (**7a/1**) and crystals in twist-boat conformation (**7a/2**), is dissolved in CH_2Cl_2 no ^{31}P NMR signals are observed at room temperature. At −40°C a single sharp resonance is apparent, which broadens upon lowering the temperature further and gradually

Table 2. Conformation and torsion angles [°] of the chelate cycles in **7a**, **8**, **9a**, **11−15**

Conformation of the chelate cycle[a]	Compound		M−2−3−4	2−3−4−5	3−4−5−6	4−5−6−M	5−6−M−2	6−M−2−3	3−2−6−5
Half-chair	**7a/1**	(2, 6 = P)	+40.6	−68.3	+66.3	−36.9	+7.6	−9.1	−1.4
Half-chair	**8**	(2, 6 = P)	+42.4	−65.7	+65.3	−42.3	+14.9	−14.7	+0.2
Half-chair	**9a**	(2, 6 = P)	+41.9	−70.7	+68.3	−37.1	+7.5	−9.6	−1.9
Chair	**11a**	(2 = P, 6 = Q)	+53.3	−58.8	+75.6	−78.4	+56.3	−49.0	+12.9
λ-twist	**7a/2**	(2, 6 = P)	+59.7	−44.4	−16.8	+62.7	−37.0	−11.2	−44.3
λ-twist	**11c**	(2 = P, 6 = Q)	+52.5	−54.2	−22.4	+82.8	−61.6	+11.1	−52.9
λ-twist	**12**	(2 = P, 6 = Q)	+64.5	−46.8	−33.6	+86.0	−51.6	−3.9	−57.7
λ-twist	**13**	(2, 6 = Q)	+70.0	−55.0	−32.5	+89.6	−51.0	−6.1	−61.7
λ-twist	**14**	(2, 6 = Q)	+78.3	−53.0	−37.1	+89.2	−44.3	−16.5	−67.0
λ-twist	**15**	(2 = P, 6 = Q)	+63.9	−45.1	−37.1	+84.5	−46.9	−6.7	−56.9

[a] A consistent numbering scheme for all the compounds as depicted below is used for the sake of easier comparison; the λ-enantiomer was considered throughout.

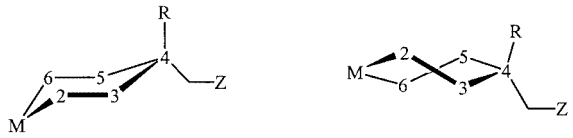

Table 3. Selected bond lengths [pm] in **7a**, **8**, **9a**, **11−15**

Coord. geometry[a]	Comp.	M, Hal	M−P	M−N	M−Hal
Square-planar	**7a/1**	Ni, Cl	216.8 (1), 217.4 (1)	−	221.1 (1), 221.3 (1)
Square-planar	**7a/2**	Ni, Cl	216.6 (1), 216.8 (1)	−	219.7 (1), 220.4 (1)
Square-planar	**8**	Ni, Br	217.8 (2), 217.8 (2)	−	234.5 (1), 236.0 (1)
Square-planar	**9a**	Pd, Cl	224.7 (2), 225.0 (2)	−	235.6 (1), 236.4 (1)
Square-planar	**12**	Pd, Cl	224.6 (1)	203.6 (2)	228.2 (1) (*trans* to N) 235.6 (1) (*trans* to P)
Tetrahedral	**11a**	Ni, Br	228.8 (1)	197.3 (1)	234.7 (1), 236.4 (1)
Tetrahedral	**11c**	Ni, Br	231.9 (2)	199.4 (5)	234.6 (1), 235.4 (1)
Tetrahedral	**13**	Ni, Cl	−	198.2 (3), 198.7 (3)	221.7 (1), 222.2 (1)
Tetrahedral	**14**	Ni, Br	−	197.7 (4), 198.4 (4)	234.8 (1), 237.9 (1)
Square-pyramidal	**15**	Ni, Br	235.9 (1)	207.0 (1)	252.6 (1) (bridged) 254.6 (1) (bridged) 245.2 (1) (terminal)

[a] Standard deviations in units of the least significant digit are given in each case.

Table 4. Selected bond angles [°] in **7a**, **8**, **9a**, **11−15**

Compd.	M, Hal	Hal−M−Hal[a]	Hal−M−P	Hal−M−N	P−M−P	P−M−N	N−M−N
7a/1	Ni, Cl	91.1(1)	86.2(1), 87.1(1), 175.2(1), 175.7(1)	−	96.0(1)	−	−
7a/2	Ni, Cl	93.0(1)	86.9(1), 88.3(1), 172.7(1), 178.0(1)	−	92.0(1)	−	−
8	Ni, Br	92.1(1)	86.1(1), 86.8(1), 174.0(1), 177.0(1)	−	95.2(1)	−	−
9a	Pd, Cl	90.0(1)	86.4(1), 88.4(1), 175.2(1), 175.8(1)	−	95.3(1)	−	−
11a	Ni, Br	124.8(1)	99.5(1), 116.7(1)	101.9(1), 113.9(1)	−	97.0(1)	−
11c	Ni, Br	124.3(1)	108.4(1), 109.4(1)	103.3(1), 112.9(1)	−	94.6(1)	−
12	Pd, Cl	90.6(1)	87.2(1), 176.9(1)	88.5(1), 178.3(1)	−	93.6(1)	−
13	Ni, Cl	125.9(1)	−	103.9(1), 105.8(1), 106.3(1), 108.3(1)	−	−	105.3(1)
14	Ni, Br	123.6(1)	−	98.7(1), 106.3(1), 108.0(1), 112.5(1)	−	−	106.8(1)
15	Ni, Br	84.4(1), 89.6(1), 154.9(3)	94.9(1), 98.1(1), 110.2(1)	88.0(1), 91.4(1), 164.0(1)	−	96.6(1)	−

[a] Standard deviations in units of the least significant digit are given in each case.

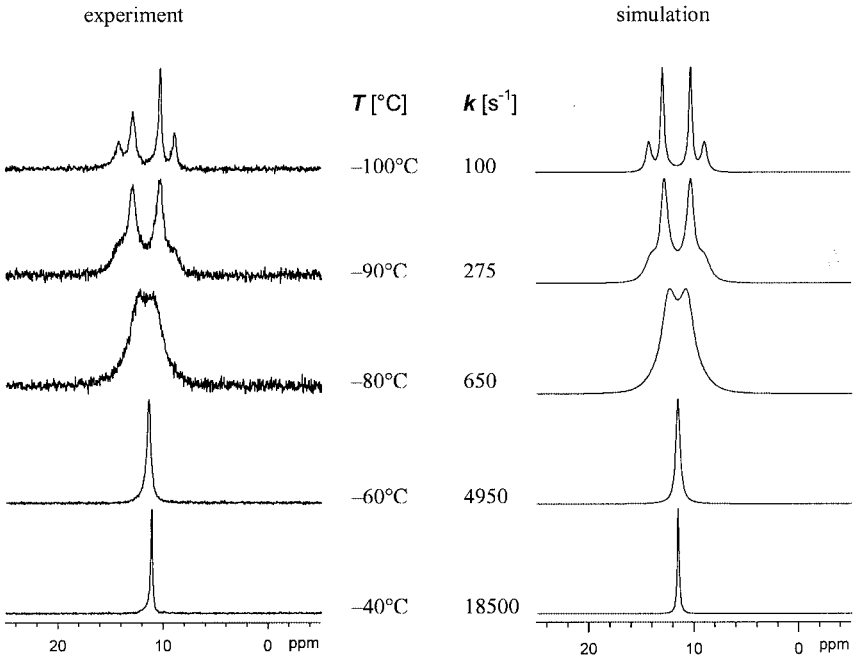

Figure 6. δ/λ isomerisation of **7a**; temperature dependence of the ^{31}P NMR spectra (81 MHz) of **7a** in CH_2Cl_2; experiment, simulation, and rate constants

evolves into a pattern corresponding to two doublets with a coupling constant of $^2J_{PP}$ = 108 Hz (Figure 6). The underlying process is interpreted in terms of a δ/λ isomerisation of the chelate cycle (Scheme 5).

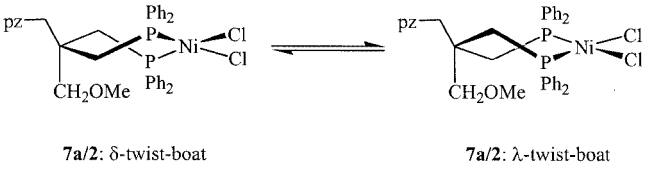

Scheme 5. δ/λ isomerisation of the chelate cycle in **7a/2**

Due to the chiral conformation of the chelate cycle the two phosphorus nuclei within the cycle in a twist conformation are no longer equivalent. A pattern of two doublets is therefore expected for the ^{31}P NMR spectrum. The observed temperature dependence of the ^{31}P NMR spectra of **7a** can be neatly simulated[13] on the hypothesis of equilibrating δ- and λ-forms of the chelate cycle. Even though **7a** has also been obtained as crystals containing the chelate cycle in a chair conformation (**7a/1**) this conformation is not observed by NMR (temperature range below −40°C), which means that in solution the chair conformation has a higher energy than the twist-boat conformation. Figure 6 shows a comparison of the observed and the simulated ^{31}P NMR spectra of **7a**.

The rate constants for the δ/λ isomerisation of **7a** (Figure 6) give a linear Eyring plot with $\Delta G^{\neq}_{298}$ = 40.2±0.5 kJ/mol, $\Delta H^{\neq}$ = 28.1±0.9 kJ/mol and $\Delta S^{\neq}$ = −40.7±5.0 J/mol K. The coalescence temperature is 200 K (81.015 MHz), which results in $\Delta G^{\neq}_{200}$ = 37.0±0.8 kJ/mol, in fair agreement with the value taken from Eyring plot analysis ($\Delta G^{\neq}_{200}$ = 37.6±0.5 kJ/mol). The activation parameters for analogous processes, involving six-membered chelate cycles containing two phosphorus donors and a rhodium(I) centre, have recently been analysed in detail.[10] The activation enthalpies are somewhat higher (around 60 kJ/mol). The activation entropies are negative throughout, around −35 J/mol K. The ^{31}P NMR pattern observed for these rhodium chelate compounds is thus − mutatis mutandis − the same as the one observed for **7a**.[10] The main difference being that the ligands in the rhodium compounds are chiral while the ligand in **7a** is not.

Nickel compounds **7b** and **7c** contain two different PR_2 groups in the chelate cycle and their ligands are therefore chiral (Table 1). It was not possible to obtain crystals suitable for X-ray analysis of these compounds. With **7b** containing a PPh_2 donor and a P(*m*-Tol)$_2$ donor the limit of slow exchange could not be reached experimentally at the lowest achievable temperature in CH_2Cl_2 (−100°C for **7b**). With the more bulky $PMes_2$ donor group in the chelate cycle of **7c** (Table 1) a ^{31}P NMR spectrum close to the slow exchange limit was evident at −90°C. The solution could be undercooled to −110°C, at which point the slow exchange limit was reached. Above 0°C, where the high temperature limit is not yet reached, paramagnetic broadening starts to obscure individual resonances.

Throughout the temperature range −30 to −110°C a pattern with two doublets ($^2J_{PP}$ = 95 Hz) persists. A second structure, which appears as a broad singlet at −30°C, evolves into a pattern composed of a pair of two doublets with coupling constants of $^2J_{PP}$ = 98 and 101 Hz (Figure 7). This type of pattern is typical for the twist-boat conformation of a chiral chelate cycle.[10] The two doublets, which do not significantly change their appearance between

−30°C and −110°C (signals at the left- and right-hand side of the spectrum depicted in Figure 7), are ascribed to the chair conformation of the chelate cycle, which is in only slow exchange with the twist-boat conformation, such that the appearance of the signals is not affected by exchange processes (Scheme 6). The thermodynamic stability of the chair and the twist-boat forms of the chelate cycle is different: the signals corresponding to the chair conformation have a 4:1 integral ratio to the signals corresponding to the twist-boat conformation at −30°C, while this ratio is only 3:2 at −110°C.

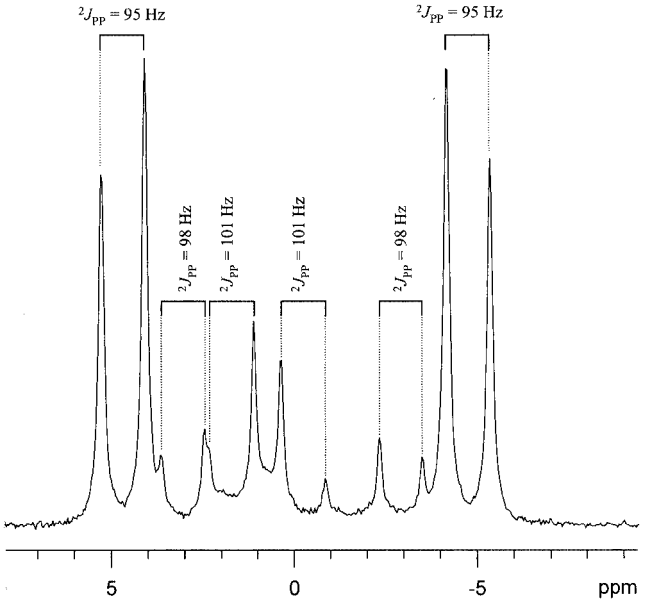

Figure 7. ^{31}P NMR spectrum of **7c** in CH_2Cl_2 at −110°C

The NMR data of **7b**−**7d** also clearly show that the ligands **5b**−**5d** bind by two phosphorus donors, with the CH_2pz group serving as a dangling arm. The structures of **7b**−**7d** are thus analogous to that of **7a** (Figure 2), which is known from crystallography (Tables 1−4). Interestingly, when the potential *tripod* ligands contain two pyrazole donors and one PR_2 donor (**6a**, **6b**) the preference for *P* coordination versus *N* coordination appears to depend on the bulkiness of the PR_2 ligand. While ligands containing one PPh_2 and two pyrazole donors show *P,N* coordination exclusively (**11a**, **11c**, **12**, **15**), ligand **6b** with a $PMes_2$,pz,pz donor set coordinates via the two pyrazole functions, with the CH_2PMes_2 group serving as a dangling arm in **13** (tetrahedral coordination). In **7c** where ligand **5c** offers a PPh_2, a $PMes_2$, and a pyrazole donor set the two phosphorus donors are bonded exclusively with the CH_2pz function playing the role of a dangling arm (square-planar coordination).

Temperature-dependent ^{1}H{^{31}P} NMR spectra of the palladium compound **12** (Figure 5) reveal a different type of dynamic exchange different to those already described. While the ^{31}P NMR signal of **12** is a singlet in the range −80 to 120°C the appearance of the proton spectrum changes drastically (Figure 8).

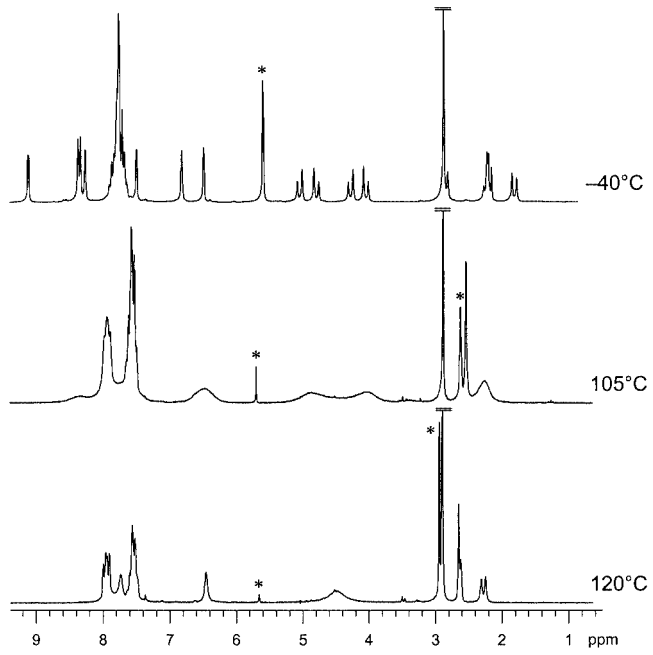

Figure 8. Variable-temperature ^{1}H{^{31}P} NMR spectra (200 MHz) of **12**; dynamic exchange is clearly apparent at δ ≈ 4.5 ppm and δ ≈ 6.5 ppm; spectra at 105 and 120°C were recorded in DMSO as solvent; at lower temperatures the solvent was CH_2Cl_2; asterisks designate solvent peaks

At −40°C a pattern of sharp signals is clearly evident, with all the resonances expected for **12** (Figure 8, Table 11). The signals corresponding to the coordinated CH_2pz arm and the noncoordinated one are clearly separated. The resonances of the coordinated pyrazole group are shifted downfield significantly (δ = 6.64, 8.98, 8.11), in contrast to the noncoordinated one (δ = 6.30, 7.33, 7.60). The methylene protons of the CH_2pz groups give rise to two doublets at δ = 3.79 and 4.02 ppm (noncoordinated) and 4.56 and 4.82 (coordinated), with similar coupling constants of about $^2J_{HH}$ = 14.5 Hz. At higher temperatures the corresponding signals coalesce. From the protons of the pyrazole groups (Table 11) only H4 (Scheme 13, Exp. Sect.) gives rise to a signal, which does not overlap with the signals of aromatic protons over the whole temperature range. Coalescence of signals of H4 for the coordinated and noncoordinated pro-

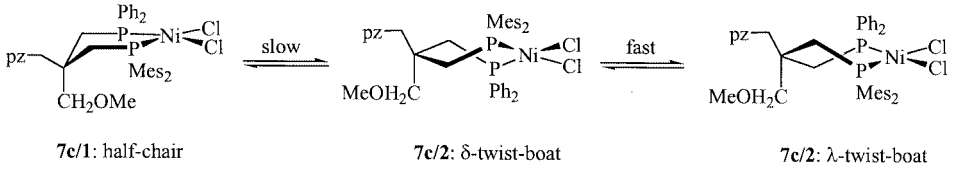

7c/1: half-chair **7c/2**: δ-twist-boat **7c/2**: λ-twist-boat

Scheme 6. Interconversion of the conformation of the chelate cycle in **7c**

ton occurs at 105°C (k_c = 350 s^{-1}), corresponding to $\Delta G^{\neq}_{378}$ = 77.5±0.8 kJ/mol. The signals of the methylene group of the CH_2pz functions (coordinated and noncoordinated) are free from overlap with other signals over the whole temperature range. Coalescence is observed at 120°C (k_c = 150 s^{-1}), corresponding to $\Delta G^{\neq}_{403}$ = 80.0±0.8 kJ/mol. This kind of exchange phenomenon (Scheme 7) has not yet been observed for potential *tripod* ligands containing a P,N,N donor set.[5b]

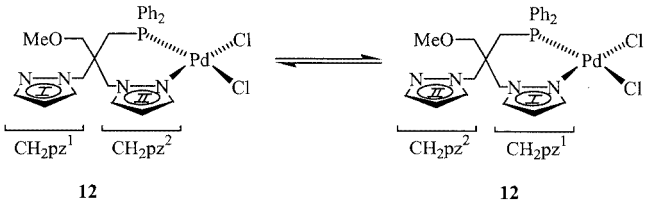

Scheme 7. Dynamic exchange of the coordinated and noncoordinated CH_2pz function of **12** at higher temperatures

Substitution Products

All compounds **7**−**14** (Table 1) contain the chelate ligands bonded to an $MHal_2$ entity. Even though the metal−halide bond lengths are independent of the type of chelate ligand within each set of compounds (square-planar, tetrahedral, see Table 3), exchange of the halide ligands by other functions might well influence the binding mode of the chelate ligand. To analyse this potential influence derivatives **16**−**19** (Scheme 8, Table 5) were synthesized in which one or both of the halide functions are replaced by organic substituents.

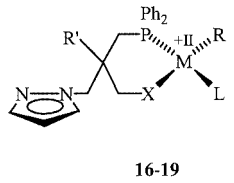

Scheme 8. General structure of **16**−**19**

Compound **7a**, after activation with $TlPF_6$, reacts with C_3H_5MgBr to produce **16a·PF$_6$** in which the phosphorus donors of the chelate cycle are *trans* to an η^3-coordinated allylic system (Scheme 9). The palladium compound **16b·PF$_6$** was obtained by treating $[Pd(\eta^3\text{-}C_3H_5)Cl]_2$ with the ligand $EtOCH_2C(CH_2PPh_2)(CH_2pz)_2$[5e] and with KPF_6 as the halide-abstracting reagent (Scheme 9).

Direct, selective substitution of just one halide function in compounds of the type $[(chelate)M^{II}Hal_2]$ was, however, not successful. Substitution products $[(chelate)M^{II}RHal]$ were synthesized by starting from $[L_2M^{II}RHal]$ [L_2 = cod, $(PPh_3)_2$] by reaction with the *tripod* ligands.

Compound **17** was obtained from [*trans*-$(PPh_3)_2$Ni(Mes)Br] using **5a** as the chelating agent (Scheme 10).

Similarly, the palladium compound **18** was obtained by the reaction of $[(\eta^4\text{-cod})PdClMe]$ with **5a** (Scheme 11).

The structures of compounds **16a·PF$_6$**, **16b·PF$_6$**, and **18** (Figure 9, Tables 6 and 9) were analysed by crystallography. Suitable single crystals could not be obtained for **17**.

When, instead of **5a**, ligand **6a** − with its two pyrazole functions − was treated with [*trans*-$(PPh_3)_2$Ni(Mes)Br] the formation of **6a·Ni(Br)Mes** as an analogue of **17** (Scheme 10) was indicated by its ^{31}P NMR spectrum (a sin-

Table 5. Substitution compounds **16**−**19**

Compd.	Ligand	Coord. group X	Noncoord. group R′	M(R)(L)	Colour of compd.	Coord. geometry	Crystal structure
16a·PF$_6$	**5a**	PPh_2	CH_2OMe	Ni(allyl)$^+$	yellow	square-planar	yes
16b·PF$_6$	−[a]	pz	CH_2OEt	Pd(allyl)$^+$	colourless	square-planar	yes
17	**5a**	PPh_2	CH_2OMe	Ni(Mes)Br	yellow	square-planar	no
18	**5a**	PPh_2	CH_2OMe	PdMeCl	pale grey	square-planar	yes
19·PF$_6$	**6a**	pz	CH_2OMe	Ni(Mes)$(PPh_3)^+$	yellow	square-planar	yes

[a] Ligand $EtOCH_2C(CH_2PPh_2)(CH_2pz)_2$; synthesis see ref.[5e]

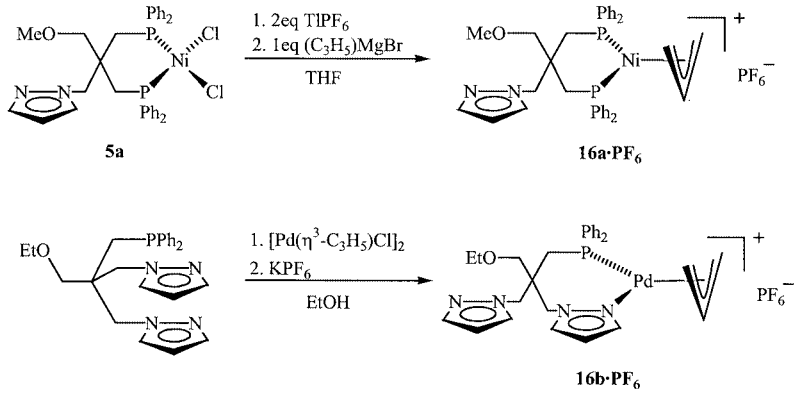

Scheme 9. Synthesis of cationic (η^3-allyl)metal complexes **16a·PF$_6$** and **16b·PF$_6$**

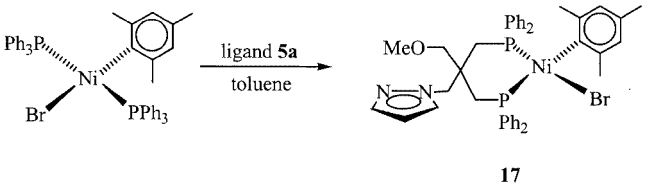

Scheme 10. Synthesis of compound **17**

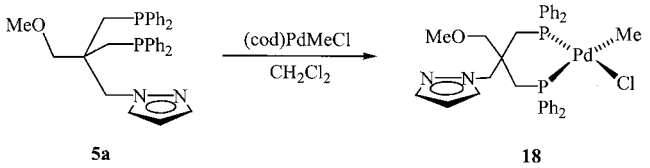

Scheme 11. Synthesis of compound **18**

glet at δ = 11.8 ppm). However, the compound could not be crystallized. Treatment of the reaction mixture with $TlPF_6$ resulted in the expected $Br^- \rightleftarrows PPh_3$ exchange to produce **19·PF$_6$** (Scheme 12), which could be characterized by X-ray analysis (Figure 10, Tables 6, 9).

The conformation of the chelate cycles (Table 6) in **16a**$^+$, **16b**$^+$, **18**, and **19**$^+$ is quantitatively similar to that described for [(chelate)$M^{II}Hal_2$] compounds (Table 2). In all four compounds the coordination around the metal atom is square-planar. The conformation of the chelate cycles (Table 6) corresponds to a chair (**16a**$^+$, **19**$^+$), a half-chair (**18**) and a twist-boat conformation (**16b**$^+$). The bond lengths between the chelate donor atoms and the metal atoms are very similar to the ones shown in Table 3. The M−C and M−Hal distances to the external ligands, as well as the valence angles at the metal centre, are all in the usual and normal range (Table 6). The only clear indication of a *trans* influence is observed for the M−P bonds in **18**. The N−P bond *trans* to the chloride ligand is not much different from the one observed in **12** (224.6 pm) with its P_2Cl_2 donor set (Table 3). The M−P distance *trans* to the methyl substituent in **18** is lengthened by the *trans* influence of the methyl group to 231.4 pm (Table 6). There is, however, some uncertainty with respect to the exact values of both distances, which may be larger than the calculated standard deviation (Table 6), due to the fact that crystals of **18** show some positional disorder between the chloride and the methyl substituents even though this disorder could be resolved by appropriate refinement (Table 9).

While the structure of the intermediate [**6a·Ni(Br)Mes**] formulated in the synthesis of **19·PF$_6$** may be − albeit indirectly − inferred from X-ray analysis of **19·PF$_6$** (see above) the structure of **17** [**5a·Ni(Br)Mes**] has to be inferred

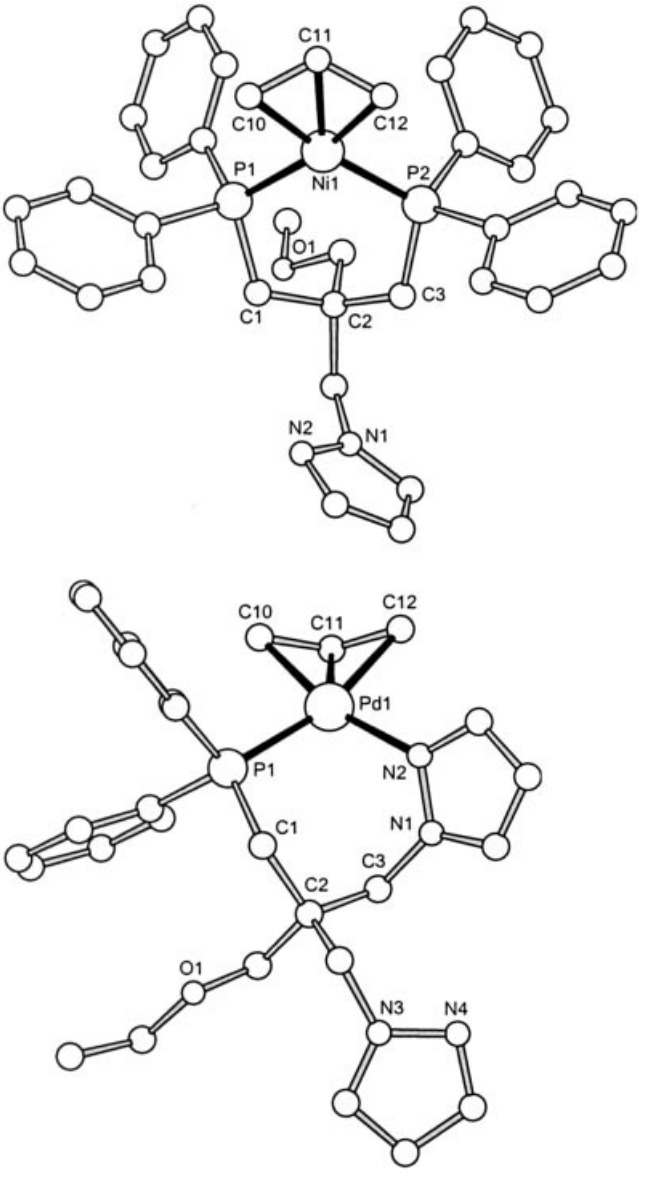

Figure 9. X-ray structure of the cation **16a**$^+$ (top) and **16b**$^+$ (bottom)

inter alia from NMR data. As expected for the diastereotopic phosphorus nuclei in **17** (the compound as a whole is chiral!) two doublets are observed in its ^{31}P NMR spectrum (see Exp. Sect. and remark therein). The diamagnetism of **17** proves the square-planar coordination of the nickel centre.

Even if the above results show that the conformation of the chelate cycles is not very much dependent on the kind

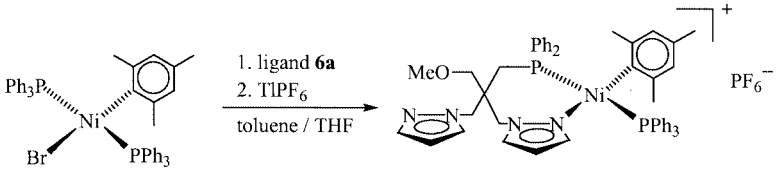

Scheme 12. Synthesis of **19·PF$_6$**

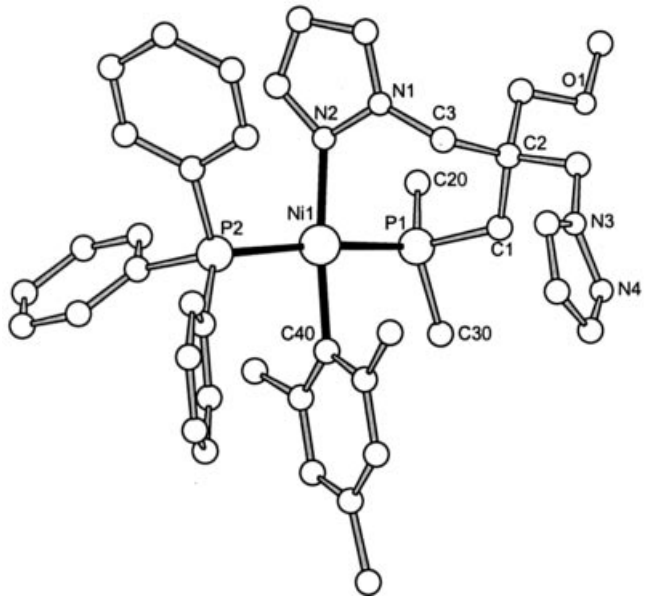

Figure 10. X-ray structure of the cation **19**$^+$ (for the sake of clarity, the phenyl groups of the *tripod* ligand are represented by their *ipso*-carbon atom only)

of co-ligands L in [(chelate)$M^{II}L_2$] there is a definite influence due to the kind of co-ligands on the type of coordination around a nickel(II) centre: ligand **6a** results in a tetrahedral coordination of the nickel atom with the $NiBr_2$ fragment (**11a**) while the same ligand coordinated to an $[Ni^{II}(PPh_3)(Mes)]^+$ fragment induces a square-planar coordination in **19**$^+$. The greater ligand field of PPh_3 and Mes (**19**$^+$) as compared with the two Br (**11a**) must be the reason for this.

Conclusion

1. The synthesis of *tripod* ligands $RCH_2C(CH_2PR_2)(CH_2pz)(CH_2X)$ with X being a phosphorus or a nitrogen donor has broad applicability.

2. These potential *tripod* ligands coordinate to d^8-metal ions (Ni^{II}, Pd^{II}, Pt^{II}) as bidentate chelate cycles, leaving the third group as a dangling arm. For ligands with a P,P,N donor set, coordination via the two phosphorus donors is generally observed. For ligands with a P,N,N donor set containing a bulky phosphorus donor (CH_2PMes_2), *N*,*N* coordination may be preferred over *P*,*N* coordination.

Table 6. Selected bond lengths [pm], bond angles [°], and torsion angles [°] of compounds **16a**, **16b**, **18**, and **19**

	16a·PF$_6$			**16b·PF$_6$**			**18**				**19·PF$_6$**			
	M	X	R, L	M	X	R, L	M	X	R	L	M	X	R	L
	Ni	PPh_2	η^3-$C_3H_5^-$	Pd	pz	η^3-$C_3H_5^-$	Pd	PPh_2	CH_3^-	Cl^-	Ni	pz	Mes^-	PPh_3
Chelate cycle[a][b]	Chair (2, 6 = P)			λ-twist (2 = P, 6 = Q)			Half-chair (2, 6 = P)				chair (2 = P, 6 = Q)			
M−2−3−4	+45.3			+60.2			+42.4				+58.6			
2−3−4−5	−62.4			−50.2			−67.3				−51.1			
3−4−5−6	+62.9			−32.1			+69.3				+65.5			
4−5−6−M	−46.7			+84.5			−45.2				−80.0			
5−6−M−2	+25.6			−53.7			+17.1				+66.8			
6−M−2−-3	−24.8			+0.9			−16.4				−61.0			
3−2−6−5	+0.7			−57.0			+0.7				+11.9			
M−C	200.8(1) (internal)			214.4(4) (internal)			218.0(3)				194.5(4) (*trans* to N)			
	202.3(1), 204.6(1) (terminal)			211.2(4) (*trans* to N)			–				–			
				220.7(3) (*trans* to P)										
M−Cl	–			–			236.3(1)				–			
M−P	217.0(2), 217.4(2)			230.0(1)			223.7(1) (*trans* to Cl^-)				222.4(3) (P = ligand)			
							231.4(1) (*trans* to CH_3^-)				225.8(3) (P = PPh_3)			
M−N	–			209.5(3)			–				196.1(7) (*trans* to Mes^-)			
P−M−R	93.5(1)			97.1(1)			88.1(1)				88.4(1)			
P−M−X	99.5(1)			96.5(1)			95.8(1)				91.0(1)			
L−M−X	94.8(1)			98.3(1)			90.1(1)				94.2(1)			
L−M−R	72.1(1)			67.8(1)			86.2(1)				87.3(1)			
L−M−P	166.4(1)			164.7(1)			173.6(1)				172.2(1)			
X−M−R	165.3(1)			165.7(1)			174.4(1)				171.6(1)			

[a] Standard deviations in units of the least significant digit are given in each case. [b] A consistent numbering scheme for all the compounds as depicted below is used for the sake of easier comparison.

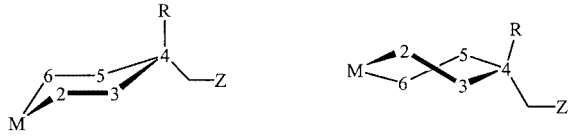

3. For palladium(II) compounds derived from ligands containing a P,N,N donor set, dynamic exchange between coordinated and noncoordinated N donors is observed.

4. While palladium(II) and platinum(II) derivatives show a square-planar coordination throughout, the kind of coordination around the nickel atom (square-planar versus tetrahedral) depends on the donor set of the chelate ligand as well as on the kind of co-ligands.

Experimental Section

General Remarks: All manipulations involving phosphanes were carried out under argon by means of standard Schlenk techniques. All solvents were dried by standard methods[14] and distilled under argon. The solvents $CDCl_3$ and CD_2Cl_2 used for NMR spectroscopic measurements were degassed by three successive freeze-pump-thaw cycles and dried over molecular sieves (4 Å). NMR: Bruker Avance DPX 200 at 200.12 MHz (^{1}H); 50.323 MHz (^{13}C{^{1}H}); 81.015 MHz (^{31}P{^{1}H}); T = 303 K unless stated otherwise; chemical shifts (δ) in ppm with respect to $CDCl_3$ (^{1}H: δ = 7.27 ppm; ^{13}C: δ = 77.0 ppm) and CD_2Cl_2 (^{1}H: δ = 5.32 ppm; ^{13}C: δ = 53.5 ppm) as internal standards. ^{31}P chemical shifts (δ) in ppm with respect to 85% H_3PO_4 (^{31}P: δ = 0 ppm) as external standard. The NMR numbering scheme for the pyrazole cycle is shown in Scheme 13.[15] MS: Finnigan MAT 8230; EI (70 eV); FAB (xenon; matrix: 4-nitrobenzyl alcohol). UV/Vis: Perkin−Elmer Lambda 19. Elemental analyses: Microanalytical Laboratory of the Organisch-Chemisches Institut, University of Heidelberg.

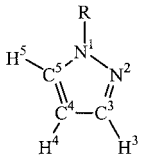

Scheme 13. Numbering scheme of pyrazole as used for NMR data

Crystallographic Structure Determinations: Suitable crystals were taken directly from the mother liquor, immersed in perfluorinated polyether oil, and fixed to a glass capillary at 200 K. The measurements were carried out with a Siemens P4 four-circle diffractometer or with an Enraf−Nonius Kappa CCD diffractometer, using graphite-monochromated Mo-K_α radiation throughout. For the Siemens P4 diffractometer measurements the intensities of three check reflections (measured every 100 reflections) remained constant throughout the data collection, thus indicating crystal and electronic stability. The data collected with the Siemens P4 diffractometer were corrected as usual, including an experimental ab-

Table 7. Crystallographic data of compounds **7a/1**, **7a/2**, **8**, **9a**, and **11a**

	7a/1	**7a/2**	**8**	**9a**	**11a**
Empirical formula (without solvate)	$C_{33}H_{34}Cl_2N_2NiOP_2$	$C_{33}H_{34}Cl_2N_2NiOP_2$	$C_{33}H_{34}Br_2N_2NiOP_2$	$C_{33}H_{34}Cl_2N_2OP_2Pd$	$C_{24}H_{27}Br_2N_4NiOP$
Formula mass [g/mol]	666.2	666.2	755.1	713.9	637.0
Solvate	1 CH_2Cl_2	0.5 CH_2Cl_2	−	1 CH_2Cl_2	−
Crystal size [mm]	0.20×0.30×0.40	0.20×0.30×0.40	0.30×0.30×0.40	0.20×0.20×0.30	0.30×0.20×0.05
Crystal system	monoclinic	triclinic	monoclinic	monoclinic	monoclinic
Space group	$P2_1/c$ (no. 14)	$P\bar{1}$ (no. 2)	$P2_1/n$ (no. 14)	$P2_1/c$ (no. 14)	$P2_1/n$ (no. 14)
Lattice constants:					
a [pm]	1136.6(3)	1140.2(3)	1110.1(3)	1144.0(2)	1082.5(2)
b [pm]	2283.6(5)	1118.0(3)	1304.6(2)	2300.8(4)	2004.4(4)
c [pm]	1359.7(6)	1609.3(3)	2211.3(4)	1367.4(2)	1168.4(2)
α [°]	90	81.27(2)	90	90	90
β [°]	93.68(2)	89.71(2)	93.41(1)	86.51(1)	92.75(3)
γ [°]	90	61.75(1)	90	90	90
V [10^6×pm^3]	3522(1)	1781(1)	3197(1)	3593(1)	2532(1)
Z	4	2	4	4	4
d_x [g×cm^{-3}]	1.417	1.320	1.569	1.473	1.671
T [K]	200	200	200	200	200
Measuring device	Siemens Nicolet-Syntex	Siemens Nicolet-Syntex	Siemens Nicolet-Syntex	Siemens Nicolet-Syntex	Nonius Kappa CCD
No. of reflect. for cell refinement	31	31	37	33	
Scan range [°]	3.5 ≤ 2Θ ≤ 54.0	4.1 ≤ 2Θ ≤ 48.0	3.6 ≤ 2Θ ≤ 51.0	3.5 ≤ 2Θ ≤ 51.0	4.0 ≤ 2Θ ≤ 55.0
Method	ω-scan, Δω = 0.54°	ω-scan, Δω =0.54°	ω-scan, Δω =0.54°	ω-scan, Δω =0.54°	ω-scan, Δω = 1.00°
Scan speed	10° min^{-1}	12° min^{-1}	12° min^{-1}	8° min^{-1}	5 s/frame
No. of measured reflections	8071	5826	6225	7030	10996
No. of unique reflections	7689	5510	5908	6681	5742
No. of observed reflections	5769	4543	3916	4626	4682
Observation criterion	$I \geq 2\sigma$	$I \geq 2\sigma$	$I \geq 2\sigma$	$I \geq 2\sigma$	$I \geq 2\sigma$
No. of param. refined	403	411	398	403	302
Resid. el. density [10^{-6}e·pm^{-3}]	0.61	0.95	0.61	0.79	0.45
R_1/R_w [%] (refinement on F^2)	4.3/13.5	4.9/15.4	4.5/12.2	5.0/11.0	3.2/7.6

Table 8. Crystallographic data of compounds **11c**, and **12**−**15**

	11c	**12**	**13**	**14**	**15**
Empirical formula (without solvate)	$C_{25}H_{29}Br_2N_4NiOP$	$C_{24}H_{27}Cl_2N_4OPPd$	$C_{30}H_{39}Cl_2N_4NiOP$	$C_{14}H_{18}Br_2N_6Ni$	$C_{50}H_{58}Br_4N_8Ni_2O_2P_2$
Formula mass [g/mol]	651.0	595.8	632.2	488.8	1302.0
Solvate	0.5 CH_2Cl_2	−	−	−	−
Crystal size [mm]	0.30×0.30×0.30	0.20×0.10×0.05	0.08×0.15×0.40	0.30×0.20×0.20	0.30×0.30×0.30
Crystal system	monoclinic	triclinic	triclinic	orthorhombic	triclinic
Space group	$P2_1/c$ (no. 14)	$P\bar{1}$ (no. 2)	$P\bar{1}$ (no. 2)	*Pbca* (no. 61)	$P\bar{1}$ (no. 2)
Lattice constants:					
a [pm]	958.4(3)	792.1(2)	790.0(2)	1418.7(3)	943.3(2)
b [pm]	1345.0(3)	852.9(2)	1225.0(3)	1486.7(3)	982.3(2)
c [pm]	2266.8(5)	1860.4(4)	1577.2(3)	1694.3(3)	1574.2(2)
α [°]	90	94.76(3)	91.48(3)	90	80.15(1)
β [°]	80.63(2)	100.88(3)	90.15(3)	90	74.09(1)
γ [°]	90	91.97(3)	97.29(3)	90	70.04(1)
V [10^6×pm^3]	2883(1)	1228(1)	1514(1)	3574(1)	1314(1)
Z	4	2	2	8	1
d_x [g×cm^{-3}]	1.600	1.611	1.387	1.817	1.646
T [K]	200	200	200	200	200
Measuring device	Siemens Nicolet-Syntex	Nonius Kappa CCD	Nonius Kappa CCD	Nonius Kappa CCD	Siemens Nicolet-Syntex
No. of reflect. for cell refinement	31				32
Scan range [°]	4.3 ≤ 2Θ ≤ 52.0	4.5 ≤ 2Θ ≤ 55.0	3.4 ≤ 2Θ ≤ 55.1	4.6 ≤ 2Θ ≤ 52.0	4.4 ≤ 2Θ ≤ 51.0
Method	ω-scan, Δω =0.54°	ω-scan, Δω =1.00°	ω-scan, Δω =1.00°	ω-scan, Δω =1.00°	ω-scan, Δω =0.54°
Scan speed	8° min^{-1}	10 s/frame	2 s/frame	10 s/frame	8° min^{-1}
No. of measured reflections	5939	7896	13724	15731	5162
No. of unique reflections	5599	5538	6951	3525	4848
No. of observed reflections	3702	4670	4260	1544	3833
Observation criterion	$I \geq 2\sigma$	$I \geq 2\sigma$	$I \geq 2\sigma$	$I \geq 2\sigma$	$I \geq 2\sigma$
No. of param. refined	341	302	362	212	312
Resid. el. density [10^{-6}e·pm^{-3}]	0.87	0.43	0.83	0.78	0.76
R_1/R_w [%] (refinement on F^2)	5.5/15.3	3.1/6.8	5.2/12.7	4.9/6.5	3.6/9.9

sorption correction. Data from the Enraf−Nonius Kappa CCD device were processed using the standard Nonius software.[16] The calculations were performed using the SHELXT PLUS software package. Structures were solved by direct methods with the SHELXS-97 program and refined with the SHELXL-97 program.[17] Graphical handling of the structural data during solution and refinement was performed with XMPA.[18] Atomic coordinates and anisotropic thermal parameters of the non-hydrogen atoms were refined by full-matrix least-squares calculations. Data relating to the structure determinations are collected in Tables 7, 8, and 9. Figures 1−5, 9, and 10 were prepared using WinRay-32.[19] CCDC-194026 to -194039 contain the supplementary crystallographic data for this paper. These data can be obtained free of charge at www.ccdc.cam.ac.uk/conts/retrieving.html [or from the Cambridge Crystallographic Data Centre, 12 Union Road, Cambridge CB2 1EZ, UK; Fax: (internat.) + 44-1223/336-033; E-mail: deposit@ccdc.cam.ac.uk].

Materials: Silica gel (Kieselgel 32−63 μm, ICN Biomedicals GmbH) used for chromatography was degassed at 1 mbar for 24 h and saturated with argon. A solution of *n*BuLi in hexane (2.5 M) was used for deprotonations. **1**,[1c] **2a**,[5e] **2c**,[5e] **3a**,[5e] **4a**,[5e] $EtOCH_2C(CH_2PPh_2)(CH_2pz)_2$,[5e] $CH_3C(CH_2pz)_3$,[5e] $HPPh_2$,[20] $HPMes_2$,[21] [*trans*-$(PPh_3)_2Ni(Mes)Br$],[22] and [(cod)PdClMe][23] were prepared according to or by adaptation of literature procedures. All other chemicals were obtained from commercial suppliers and used without further purification. Boiling range of the light petroleum ether used: 40−60°C. NMR and analytical data are collected in Tables 10−15.

Ligand Synthesis

Synthesis of 2b: Pyrrole (0.81 g, 12 mmol) was dissolved in THF (50 mL) and deprotonated at 0°C with 1 equiv. of KO*t*Bu (1.35 g, 12 mmol). After warming to 25°C, the solution was stirred for 30 min and then added at 0°C to a solution of **1** (2.59 g, 10 mmol) in THF (50 mL). The reaction was completed by refluxing for 4 h. In another flask, $HPPh_2$ (2.23 g, 12 mmol) was dissolved in THF (50 mL) and deprotonated at 0°C with 1 equiv. of KO*t*Bu (1.35 g, 12 mmol). After warming to 25°C and stirring for 30 min, the red potassium phosphide solution was added dropwise to the first reaction mixture, which was maintained at 0°C. After warming to 25°C and stirring for 10 h (the phosphide substitution was monitored by TLC), the then yellow solution was quenched by the addition of deoxygenated water (20 mL). The aqueous phase was extracted with diethyl ether (30 mL, 2×). The combined organic phases were washed with deoxygenated brine, dried with $MgSO_4$, filtered, and concentrated in vacuo. The resulting viscous oil was purified by column chromatography on silica gel by using petroleum ether/diethyl ether (1:1; R_f = 0.47) as eluent to obtain 1.84 g (5.5 mmol, 55%) of **2b** as a colourless, microcrystalline powder. ^{31}P NMR ($CDCl_3$): δ = −26.9 (s, PPh_2) ppm. For further analytical data see Tables 10, 12, and 14.

General Procedure for the Synthesis of 3 and 4 The appropriately substituted oxetane **2** (1 equiv.) was dissolved in THF (50 mL). In a second flask, HPR_2 (1.2 equiv.) was dissolved in THF (50 mL) and deprotonated at 0°C with *n*BuLi (1.2 equiv.). After warming to 25°C and stirring for 30 min, the red lithium phosphide solution

Table 9. Crystallographic data of compounds **16a**, **16b**, **18**, and **19**

	16a·PF$_6$	**16b·PF$_6$**	**18**	**19·PF$_6$**
Empirical formula (without solvate)	$C_{36}H_{39}F_6N_2NiOP_3$	$C_{28}H_{34}F_6N_4OP_2Pd$	$C_{34}H_{37}ClN_2OP_2Pd$	$C_{51}H_{53}F_6N_4NiOP_3$
Formula mass [g/mol]	781.3	725.0	693.5	1003.6
Solvate	0.75 CH_2Cl_2	–	–	0.35 CH_2Cl_2
Crystal size [mm]	0.30×0.30×0.40	0.05×0.05×0.30	0.20×0.10×0.05	0.10×0.05×0.05
Crystal system	monoclinic	orthorhombic	monoclinic	triclinic
Space group	*Cc* (no. 9)	*Pna*2$_1$ (no. 33)	*P*2$_1$/*n* (no. 14)	*P*$\bar{1}$ (no. 2)
Lattice constants:				
a [pm]	1706.3(3)	1947.8(4)	1110.9(2)	1091.5(2)
b [pm]	1207.7(2)	1712.2(3)	1328.7(3)	1186.1(2)
c [pm]	1875.0(5)	898.3(2)	2174.2(4)	2098.4(4)
α [°]	90	90	90	91.25(3)
β [°]	95.80(1)	90	91.70(3)	105.04(3)
γ [°]	90	90	90	111.04(3)
V [10^6×pm^3]	3844(1)	2996(1)	3208(1)	2429(1)
Z	4	4	4	2
d_x [g×cm^{-3}]	1.460	1.607	1.430	1.412
T [K]	200	200	200	200
Measuring device	Siemens Nicolet-Syntex	Nonius Kappa CCD	Nonius Kappa CCD	Nonius Kappa CCD
No. of reflect. for cell refinement	25			
Scan range [°]	4.1 ≤ 2Θ ≤ 51.0	3.2 ≤ 2Θ ≤ 52.0	3.7 ≤ 2Θ ≤ 55.0	3.7 ≤ 2Θ ≤ 50.0
Method	ω-scan, Δω =0.54°	ω-scan, Δω =1.00°	ω-scan, Δω =1.00°	ω-scan, Δω =0.50°
Scan speed	12° min^{-1}	30 s/frame	30 s/frame	30 s/frame
No. of measured reflections	3430	43721	13378	16851
No. of unique reflections	3430	5882	7316	8526
No. of observed reflections	2772	5315	5458	5380
Observation criterion	$I \geq 2\sigma$	$I \geq 2\sigma$	$I \geq 2\sigma$	$I \geq 2\sigma$
No. of param. refined	477	399	375	548
Resid. el. density [10^{-6}e·pm^{-3}]	0.44	0.39	0.62	1.02
R_1/R_w [%] (refinement on F^2)	5.3/14.6	2.8/6.3	5.5/10.0	14.6/24.3

was added dropwise to the oxetane solution at 0°C. The mixture was allowed to warm to 25°C, while the reaction progress was monitored by TLC. Upon completion (10 h stirring at 25°C), the reaction was quenched by the addition of deoxygenated water (50 mL). The aqueous phase was extracted with diethyl ether (30 mL, 2×). The combined organic phases were washed with deoxygenated brine, dried with $MgSO_4$, filtered, and concentrated in vacuo yielding the crude products as pale yellow oils. The crude product was purified by column chromatography on silica gel. **3b**: Starting material **2a** (2.02 g, 6.0 mmol). Eluent petroleum ether/diethyl ether (2:1; R_f = 0.24). Yield 1.90 g (3.45 mmol, 58%) as a colourless, microcrystalline powder. ^{31}P NMR ($CDCl_3$): δ = −29.9 [d, $^4J_{PP}$ = 10 Hz, *P*(*m*-Tol)$_2$], −29.5 (d, $^4J_{PP}$ = 10 Hz, *P*Ph$_2$) ppm. **3c**: Starting material **2a** (1.97 g, 5.85 mmol). Eluent petroleum ether/diethyl ether (1:1; R_f = 0.51). Yield 2.89 g (4.75 mmol, 81%) as a colourless, microcrystalline powder. ^{31}P NMR ($CDCl_3$): δ = −35.9 (d, $^4J_{PP}$ = 16 Hz, *P*Mes$_2$), −28.3 (d, $^4J_{PP}$ = 16 Hz, *P*Ph$_2$). **3d**: Starting material **2a** (2.02 g, 6.0 mmol). Eluent petroleum ether/diethyl ether (3:1; R_f = 0.35). Yield 1.35 g (2.5 mmol, 42%) as a colourless, microcrystalline powder. ^{31}P NMR ($CDCl_3$): δ = −29.9 (br. s, *P*Ph$_2$), −18.5 [br. s, *P*(*c*-C_6H_{11})$_2$] ppm. **3e**: Starting material **2b** (670 mg, 2.0 mmol). Eluent petroleum ether/diethyl ether (2:1, R_f = 0.36). Yield 830 mg (1.6 mmol, 80%) as a colourless, microcrystalline powder. ^{31}P NMR ($CDCl_3$): δ = −29.5 (s, *P*Ph$_2$) ppm. **4b**: Starting material **2c** (1.75 g, 8.0 mmol). Eluent petroleum ether/diethyl ether (2:3; R_f = 0.35). Yield 2.65 g (5.4 mmol, 68%) as a colourless, microcrystalline powder. ^{31}P NMR ($CDCl_3$): δ = −36.5 (s, *P*Mes$_2$) ppm. For further analytical data see Tables 10, 12, and 14.

General Procedure for the Synthesis of 5 and 6: The substituted hydroxy compound **3** or **4** (1 equiv.), respectively, was dissolved in THF (50 mL) and the solution was cooled to 0°C. Addition of solid KO*t*Bu (2 equiv.) yielded a clear, pale yellow solution. After 5 min of stirring at 0°C, 2 equiv. of methyl iodide was added rapidly. Within a few minutes KI precipitated. The suspension was stirred for at 0°C 1 h (the methylation was monitored by TLC). The solvent was evaporated in vacuo at 0°C. The residue was dissolved in diethyl ether (30 mL) and the solution was filtered to remove potassium iodide. Removal of the solvent yielded the crude products as colourless oils. The crude product was purified by column chromatography on silica gel. **5a**: Starting material **3a** (1.77 g, 3.4 mmol). Eluent petroleum ether/diethyl ether (3:1; R_f = 0.36). Yield 1.41 g (2.6 mmol, 78%) as a colourless, microcrystalline powder. ^{31}P NMR ($CDCl_3$): δ = −28.7 (s, *P*Ph$_2$) ppm. **5b**: Starting material **3b** (1.60 g, 2.9 mmol). Eluent petroleum ether/diethyl ether (3:1; R_f = 0.36). Yield 1.31 g (2.3 mmol, 80%) as a colourless, microcrystalline powder. ^{31}P NMR ($CDCl_3$): δ = −29.0 [d, $^4J_{PP}$ = 6 Hz, *P*(*m*-Tol)$_2$], −28.7 (d, $^4J_{PP}$ = 6 Hz, *P*Ph$_2$) ppm. **5c**: Starting material **3c** (700 mg, 1.15 mmol). Eluent petroleum ether/diethyl ether (3:1; R_f = 0.43). Yield 615 mg (1.0 mmol, 87%) as a colourless, microcrystalline powder. ^{31}P NMR ($CDCl_3$): δ = −35.8 (d, $^4J_{PP}$ = 6 Hz, *P*Mes$_2$), −28.3 (d, $^4J_{PP}$ = 6 Hz, *P*Ph$_2$). **5d**: Starting material **3e** (625 mg, 1.2 mmol). Eluent petroleum ether/diethyl ether (2:1; R_f = 0.65). Yield 560 mg (1.05 mmol, 87%) as a colourless, microcrystalline powder. ^{31}P NMR ($CDCl_3$): δ = −29.2 (s, *P*Ph$_2$) ppm. **6a**: Starting material **4a** (1.62 g, 4.0 mmol). Eluent petroleum ether/diethyl ether (2:1; R_f = 0.49). Yield 1.49 g (3.6 mmol, 89%) as a colourless, microcrystalline powder. ^{31}P

Table 10. Chemical shifts (δ values), integrals [*x* H] and coupling constants *J* in the $^1H\{^{31}P\}$ NMR spectra of **2**−**6** in $CHCl_3$

Compd.[a][b]	CH_2N [2 H]	CH_2O [2 H]	CH_2P [4 H]	OH [1 H]	OCH_3 [3 H]	Pyrazole-H[c] H4[d] [1 H]	H5[d] [1 H]	H3[d] [1 H]	Aryl-H	Other
2b	4.48 s	4.30 d, 4.42 d [4 H] $^2J_{HH}$ = 6.2	2.44 s [2 H]	–	–	–	–	–	7.36−7.51 m [10 H]	6.19 pt, 6.72 pt [4 H] pyrrole-*H*[c]
3a	4.23 s	3.26 s	2.46 br. s	n. d.	–	6.18 t	7.09 d	7.49 d	7.33−7.46 m [20 H]	
3b	4.28 s	3.31 s	2.49 br. s	4.06 br. s	–	6.21 t	7.15 d	7.50 d	7.22−7.49 m [18 H]	2.35 br. s [6 H] *m*-C*H*$_3$
3c	4.13 d, 4.26 d $^2J_{HH}$ = 14.2	3.23 d, 3.36 d $^2J_{HH}$ = 12.0	2.49 m, 2.72 d, 2.86 d $^2J_{HH}$ = 14.3	3.92 br. s	–	6.16 t	6.90 d	(o)	6.78 m [4 H], 7.29−7.48 m [10 H]	2.24 s [6 H] *p*-C*H*$_3$ 2.38 s, 2.40 s [12 H] *o*-C*H*$_3$
3d	4.29 br. s	3.30 d, 3.46 d $^2J_{HH}$ = 11.8	1.73 m, 2.33 d, 2.46 d $^2J_{HH}$ = 14.7	4.22 br. s	–	6.24 t	(o)	(o)	7.30−7.52 m [10 H]	1.21 m, 1.48 m, 1.73 m [22 H] cyclohexyl-*H*
3e	4.11 s	3.43 s	2.24 d, 2.39 d $^2J_{HH}$ = 14.3	n. d.	–	–	–	–	7.28−7.51 m [20 H]	6.12 pt, 6.69 pt [4 H] pyrrole-*H* [c]
4a	4.22 d, 4.46 d [4 H] $^2J_{HH}$ = 14.3	3.27 s	2.13 s [2 H]	4.37 br. s	–	6.26 t [2 H]	7.31 d [2 H]	7.60 d [2 H]	7.35−7.48 m [10 H]	
4b	4.24 d, 4.38 d [4 H] $^2J_{HH}$ = 14.3	3.33 s	2.55 s [2 H]	4.01 br. s	–	6.22 t [2 H]	7.38 d [2 H]	7.54 d [2 H]	6.83 m [4 H]	2.26 s [6 H] *p*-C*H*$_3$ 2.40 br. s [12 H] *o*-C*H*$_3$
5a	4.44 s	3.03 s	2.51 br. s	–	2.80 s	6.24 t	(o)	7.56 d	7.32−7.48 m [20 H]	
5b	4.44 s	3.04 s	2.48 m	–	2.81 s	6.24 t	7.13 d	7.55 d	7.22−7.43 m [18 H]	2.33 s, 2.35 s [6 H] *m*-C*H*$_3$
5c	4.36 d, 4.45 d $^2J_{HH}$ = 14.0	3.00 d, 3.16 d $^2J_{HH}$ = 9.2	2.38 br. s, 2.54 d, 2.77 br. s $^2J_{HH}$ = 14.6	–	2.77 s	6.19 t	(o)	7.51 d	6.76 m [4 H], 7.28−7.50 m [10 H]	2.21 s [6 H] *p*-C*H*$_3$ 2.34 s, 2.48 s [12 H] *o*-C*H*$_3$
5d	4.14 s	2.99 s	2.42 br. s	–	2.80 s	–	–	–	7.31−7.46 m [20 H]	6.12 pt, 6.62 pt [4 H] pyrrole-*H* [c]
6a	4.32 d, 4.43 d [4 H] $^2J_{HH}$ = 14.2	3.03 s	2.23 s [2 H]	–	2.92 s	6.28 t [2 H]	7.58 d [2 H]	7.71 d [2 H]	7.33−7.50 m [10 H]	
6b	4.34 d, 4.43 d [4 H] $^2J_{HH}$ = 14.2	3.11 s	2.66 s [2 H]	–	3.03 s	6.25 t [2 H]	7.55 br. s [2 H]	7.55 br. s [2 H]	6.82 m [4 H]	2.26 s [6 H] *p*-C*H*$_3$ 2.42 br. s [12 H] *o*-C*H*$_3$

[a] s = singlet; d = doublet; t = triplet; m = multiplet; br. s = broad signal; pt = pseudo triplet; (o) = overlapped; n. d. = not detected. [b] Coupling constants in Hz. [c] Coupling constant $^3J_{HH}$ = 2.0 Hz. [d] See Scheme 13 for numbering scheme of the pyrazole.

NMR ($CDCl_3$): δ = −28.6 (s, *P*Ph$_2$) ppm. **6b**: Starting material **4b** (1.95 g, 4.0 mmol). Eluent petroleum ether/diethyl ether (2:1; R_f = 0.65). Yield 1.65 g (3.3 mmol, 82%) as a colourless, microcrystalline powder. ^{31}P NMR ($CDCl_3$): δ = −36.6 (s, *P*Mes$_2$) ppm. For further analytical data see Tables 10, 12, and 14.

Coordination Chemistry

General Procedure for the Synthesis of 7a−d: A solution of the respective *tripod* ligand **5** (1.05 mmol) in ethanol (10 mL) was added rapidly to a solution of $NiCl_2{\cdot}6H_2O$ (240 mg, 1.0 mmol) in ethanol (10 mL). The colour of the reaction mixture changed immediately to red and within a few minutes the nickel complexes precipitated. After stirring at 25°C for 1 h, the precipitate was filtered off, washed with 10-mL portions of diethyl ether (3×), and dried in vacuo. **7a**: Starting material **5a** (565 mg). Yield 540 mg (0.85 mmol, 85%) as an orange-coloured microcrystalline solid. Recrystallization from CH_2Cl_2/Et_2O afforded two different kinds of red crystals (**7a/1**·CH_2Cl_2 and **7a/2**·0.5CH_2Cl_2), both suitable for X-ray structure analysis. ^{31}P NMR (CD_2Cl_2, −30°C): δ = 11.2 (s, *P*Ph$_2$) ppm. ^{31}P NMR (CD_2Cl_2, −100°C): δ = 9.6 (d, $^2J_{PP}$ = 108 Hz, *P*Ph$_2$), 13.6 (d, $^2J_{PP}$ = 108 Hz, *P*Ph$_2$) ppm. **7b**: Starting material **5b** (590 mg). Yield 500 mg (0.72 mmol, 72%) as an orange-coloured, microcrystalline solid. ^{31}P NMR (CD_2Cl_2, −30°C): δ = 11.3 [br. s, *P*Ph$_2$, *P*(*m*-Tol)$_2$] ppm. ^{31}P NMR (CD_2Cl_2, −100°C): δ = 9.4 (d, $^2J_{PP}$ = 110 Hz), 12.1−15.0 (m) ppm. **7c**: Starting material **5c** (650 mg). Yield 710 mg (0.95 mmol, 95%) as a ruby-coloured, microcrystalline solid. ^1H NMR and ^{13}C NMR: due to dynamic processes, no sharp signals could be detected. ^{31}P NMR (CD_2Cl_2, −30°C): δ = −6.6 (d, $^2J_{PP}$ = 95 Hz, chair-*P*Mes$_2$), −0.5 (br. s, twist-*P*Mes$_2$, twist-*P*Ph$_2$), 2.2 (d, $^2J_{PP}$ = 95 Hz, chair-*P*Ph$_2$) ppm. ^{31}P NMR (CD_2Cl_2, −100°C): δ = −4.8 (d, $^2J_{PP}$ = 95 Hz, chair-*P*Mes$_2$), −3.0 (d, $^2J_{PP}$ = 98 Hz, twist-*P*Mes$_2$), −0.2 (d,

Table 11. Chemical shifts (δ values), integrals [*x* H] and coupling constants *J* in the $^1H\{^{31}P\}$ NMR spectra of **7**−**18** in CH_2Cl_2

Compd.[a][b]	CH_2N [2 H]	CH_2O [2 H]	CH_2P [4 H]	OCH_3 [3 H]	Pyrazole-H[c] H4[d] [1 H]	H5[d] [1 H]	H3[d] [1 H]	Aryl-H	Other
7a	3.82 s	1.98 s	2.26 d, 2.92 br. s $^2J_{HH}$ = 15.2	2.45 s	6.22 t	7.20 d	7.47 d	7.57−8.32 m [20 H]	
7b	3.82 s	1.96 d, 2.03 d $^2J_{HH}$ = 9.6	2.28 d, 2.30 d, 2.97 br. s $^2J_{HH}$ = 15.2	2.52 s	6.23 t	7.21 d	(o)	7.38−8.35 m [18 H]	2.51 br. s [6 H] *m*-C*H*$_3$
7d	3.66 s	2.24 s	2.08 d, 4.01 br. s $^2J_{HH}$ = 14.8	2.39 s	−	−	−	7.44−8.42 m [20 H]	6.09 pt, 6.43 pt [4 H] pyrrole-*H* [c]
8	3.74 s	1.88 s	2.50−2.60m	2.58 s	6.19 t	7.16 d	7.44 d	7.44−8.28 m [20 H]	
9a	4.07 s	2.09 s	2.33 d, 2.89 d $^2J_{HH}$ = 15.1	2.24 s	6.25 t	7.23 d	(o)	7.53−8.24 m [20 H]	
9b	4.02 s	1.99 d, 2.08 d $^2J_{HH}$ = 9.8	2.33 br. s, 2.81 d, 2.82 d $^2J_{HH}$ = 15.3	2.25 s	6.21 t	7.20 d	7.60 d	7.38−8.17 m [18 H]	2.43 br. s [6 H] *m*-C*H*$_3$
10	4.01 s	2.12 s	2.44 d, 2.94 d $^2J_{HH}$ = 15.3	2.25 s	6.24 t	7.23 d	(o)	7.52−8.21 m [20 H]	
12[e]	3.79 d[f], 4.02 d[f] [2 H] 4.56 d[g], 4.82 d[g] [2 H] $^2J_{HH}$ = 14.4[f], 14.8[g]	1.89 d, 1.96 d $^2J_{HH}$ = 9.6	1.51 d, 2.49−2.64 m [2 H] $^2J_{HH}$ = 14.4	2.59 s	6.30 t[f] [1 H] 6.64 t[g] [1 H]	7.33 d[f] [1 H] 8.98 d[g] [1 H]	7.60 d[f] [1 H] 8.11 d[g] [1 H]	7.51−8.25 m [10 H]	
16a·PF$_6$	4.19 s	2.32 s	2.52 d, 2.99 d $^2J_{HH}$ = 15.2	2.15 s	6.26 t	7.36 d	7.54 d	7.35−7.63 m [20 H]	2.15 br. s, 4.07 br. s [4 H] C*H*$_2$ 5.56 m [1 H] allyl-C*H*
17	3.84 s	2.30 d, 2.68 d $^2J_{HH}$ = 9.6	1.90−1.99 m, 2.36−2.47 m, 2.95 m	2.62 s	6.24 t	7.24 d	7.48 d	6.09−6.13 m [2 H], 7.09−8.22 m [20 H]	1.99 s [3 H] *p*-C*H*$_3$ 2.79 s, 2.83 s [6 H] *o*-C*H*$_3$
18[e]	4.06 pt $^2J_{HH}$ = 14.0	2.12 d, 2.46 d $^2J_{HH}$ = 9.6	2.00−2.31 m, 2.89 pt, 3.09 pt $^2J_{HH}$ = 14.2, 15.4	2.21 s	6.22 t	7.17 d	(o)	7.40−8.18 m [20 H]	0.67 s[h] [3 H] Pd-C*H*$_3$

[a] s = singlet; d = doublet; t = triplet; m = multiplet; br. s = broad signal; pt = pseudo triplet; (o) = overlapped. [b] Coupling constants in Hz. [c] Coupling constant $^3J_{HH}$ = 2.0 Hz. [d] See Scheme 13 for numbering scheme of the pyrazole. [e] Measuring temperature −40°C. [f] Noncoordinated CH_2pz group. [g] Coordinated CH_2pz group. [h] In ^1H NMR spectra: δ = 0.67 (dd, $^3J_{PH}$ = 3.8 and 7.8 Hz).

$^2J_{PP}$ = 101 Hz, twist-*P*Mes$_2$), 1.8 (d, $^2J_{PP}$ = 101 Hz, twist-*P*Ph$_2$), 3.1 (d, $^2J_{PP}$ = 98 Hz, twist-*P*Ph$_2$), 4.8 (d, $^2J_{PP}$ = 95 Hz, chair-*P*Ph$_2$) ppm, see Figure 7. **7d**: Starting material **5d** (560 mg). Yield 630 mg (0.95 mmol, 95%) as an orange-coloured, microcrystalline solid. ^{31}P NMR (CD_2Cl_2, −30°C): δ = 9.8 (s, *P*Ph$_2$) ppm. ^{31}P NMR (CD_2Cl_2, −100°C): δ = 10.4−10.8 (m, *P*Ph$_2$) ppm. For crystallographic data see Table 7; for further analytical data see Tables 11, 13, and 15.

General Procedure for the Synthesis of 8, 11a−c, 13, and 14: A solution of the respective *tripod* ligand **5** or **6** (1.05 mmol) in THF (20 mL) was added rapidly to a suspension of [(dme)NiCl$_2$] (220 mg, 1.0 mmol) or [(dme)NiBr$_2$] (310 mg, 1.0 mmol), respectively, in THF (20 mL). After stirring at 25°C for 12 h, all volatiles were removed in vacuo. The residual solid was washed with 10-mL portions of diethyl ether (3×) and dried in vacuo. **8**: Starting materials **5a** (565 mg) and [(dme)NiBr$_2$]. Yield 515 mg (0.68 mmol, 68%) as a red, microcrystalline solid. Recrystallization from CH_2Cl_2/Et_2O afforded red crystals suitable for X-ray structure analysis. ^{31}P NMR (CD_2Cl_2, −30°C): δ = 10.7 (s, *P*Ph$_2$) ppm. **11a**: Starting materials **6a** (440 mg) and [(dme)NiBr$_2$]. Yield 580 mg (0.91 mmol, 91%) as a blue-violet, microcrystalline solid. Recrystallization from CH_2Cl_2/Et_2O afforded blue-violet crystals suitable for X-ray structure analysis. UV/Vis (CH_2Cl_2): λ (ε) = 552 nm (200 $M^{-1}\cdot cm^{-1}$), 912 (110), 1007 (sh, 70). NMR: no NMR signals due to paramagnetism. **11b**: Starting materials **6a** (440 mg) and [(dme)NiCl$_2$]. Yield 485 mg (0.88 mmol, 88%) as a violet, microcrystalline solid. UV/Vis (CH_2Cl_2): λ (ε) = 527 nm (180 $M^{-1}\cdot cm^{-1}$), 890 (100), 997 (80). NMR: no NMR signals due to paramagnetism. **11c**: Starting materials EtOCH$_2$C(CH$_2$PPh$_2$)(CH$_2$pz)$_2$[5e] (455 mg) and [(dme)-NiBr$_2$]. Yield 525 mg (0.80 mmol, 80%) as a blue-violet, microcrystalline solid. Recrystallization from CH_2Cl_2/Et_2O afforded two different kinds of crystals, both suitable for X-ray structure analysis, which were identified as **11c**·0.5CH_2Cl_2 (blue-violet) and the dimer **15** (red-brown). UV/Vis (**11c**, CH_2Cl_2): λ (ε) = 550 nm (195 $M^{-1}\cdot cm^{-1}$), 913 (120), 1109 (sh, 50). NMR: no NMR signals due to paramagnetism. **13**: Starting materials **6b** (525 mg) and [(dme)Ni-Cl$_2$]. Yield 495 mg (0.78 mmol, 78%) as a blue-violet, microcrystalline solid. Recrystallization from CH_2Cl_2/Et_2O afforded blue-violet crystals suitable for X-ray structure analysis. UV/Vis (CH_2Cl_2): λ (ε) = 520 nm (100 $M^{-1}\cdot cm^{-1}$), 579 (140), 974 (60). NMR: no NMR signals due to paramagnetism. **14**: Starting materials

Table 12. Chemical shifts (δ values) and coupling constants J in the $^{13}C\{^1H\}$ NMR spectra of **2**−**6** in $CHCl_3$

Compd.[a][b]	CH_2N	CH_2O	CH_2P	OCH_3	C_q	Pyrazole-C C4[c]	C5[c]	C3[c]	Aryl-C	Other
2b	55.3 d $^3J_{CP}$ = 10.1	79.7 d $^3J_{CP}$ = 9.6	34.4 d $^1J_{CP}$ = 16.6	–	44.6 d $^2J_{CP}$ = 13.6	–	–	–	129.0−138.9 m	108.7, 121.9 pyrrole-*C*
3a	58.4 m	68.8 m	35.0 m	–	46.7 m	105.5	131.7	139.3	128.9−139.3 m	
3b	58.4 t $^3J_{CP}$ = 9.7	68.9 t $^3J_{CP}$ = 8.8	35.5 m	–	45.5 t $^2J_{CP}$ = 11.5	105.4	131.8	139.8	128.7−140.0 m	21.9 *m*-CH_3
3c	57.6 t $^3J_{CP}$ = 8.7	68.6 dd $^3J_{CP}$ = 8.3, 10.1	31.9 dd, 34.6 dd $^1J_{CP}$ = 17.5, 19.3 $^3J_{CP}$ = 9.2, 10.1	–	46.3 dd $^2J_{CP}$ = 12.0, 15.6	105.4	131.6	139.7	128.6−143.4 m	21.2 d *p*-CH_3 $^5J_{CP}$ = 1.8 23.7 d, 23.9 d *o*-CH_3 $^3J_{CP}$ = 13.8
3d	58.7 t $^3J_{CP}$ = 9.9	69.1 t $^3J_{CP}$ = 8.6	26.8−35.1 m	–	44.2 t $^2J_{CP}$ = 12.4	105.5	131.8	139.7	128.8−140.1 m	26.8−35.1 m cyclohexyl-*C*
3e	54.8 t $^3J_{CP}$ = 8.1	67.9 t $^3J_{CP}$ = 8.3	35.1 dd $^1J_{CP}$ = 18.1, $^3J_{CP}$ = 9.5	–	45.3 t $^2J_{CP}$ = 11.1	–	–	–	128.9−139.5 m	108.3, 123.0 pyrrole-*C*
4a	54.9 m	65.5 m	32.1 m	–	46.7 m	105.6	132.3	140.0	128.9−139.8 m	
4b	55.2 d $^3J_{CP}$ = 9.6	65.8 d $^3J_{CP}$ = 10.0	29.7 d $^1J_{CP}$ = 20.1	–	47.2 d $^2J_{CP}$ = 15.1	105.7	132.0	139.9	130.9−143.0 m	21.2 *p*-CH_3 23.8 d *o*-CH_3 $^3J_{CP}$ = 13.6
5a	57.6 t $^3J_{CP}$ = 9.3	76.8 t $^3J_{CP}$ = 8.6	35.4 dd $^1J_{CP}$ = 18.5, $^3J_{CP}$ = 9.5	58.3	44.3 t $^2J_{CP}$ = 12.0	105.5	131.5	139.4	128.7−140.0 m	
5b	57.6 t $^3J_{CP}$ = 9.2	76.8 t $^3J_{CP}$ = 8.5	35.2 m	58.3	44.3 t $^2J_{CP}$ = 12.0	105.4	131.5	139.3	128.5−140.0 m	21.8 *m*-CH_3
5c	57.6 t $^3J_{CP}$ = 9.2	77.1 m	32.6−34.7 m	58.5	45.2 dd $^2J_{CP}$ = 11.0, 15.6	105.4	131.4	139.3	128.5−143.1 m	21.2 *p*-CH_3 23.7 d, 23.9 d *o*-CH_3 $^3J_{CP}$ = 13.8
5d	55.3 t $^3J_{CP}$ = 8.7	76.6 t $^3J_{CP}$ = 8.3	35.0 dd $^1J_{CP}$ = 19.3, $^3J_{CP}$ = 11.0	58.2	44.4 t $^2J_{CP}$ = 12.0	–	–	–	128.7−140.0 m	108.1, 123.0 pyrrole-*C*
6a	54.8 d $^3J_{CP}$ = 8.6	74.1 d $^3J_{CP}$ = 8.1	32.0 d $^1J_{CP}$ = 18.1	58.6	45.6 d $^2J_{CP}$ = 12.1	105.5	132.2	139.8	128.8−139.9 m	
6b	55.0 d $^3J_{CP}$ = 10.6	74.2 d $^3J_{CP}$ = 9.6	28.9 d $^1J_{CP}$ = 19.1	58.8	46.1 d $^2J_{CP}$ = 15.6	105.5	132.0	139.6	130.7−143.1 m	21.2 *p*-CH_3 23.8 d *o*-CH_3 $^3J_{CP}$ = 14.0

[a] All signals are singlets unless otherwise stated; d = doublet; dd = doublet of doublet; t = triplet; m = multiplet. [b] Coupling constants in Hz. [c] See Scheme 13 for numbering scheme of the pyrazole.

$CH_3C(CH_2pz)_3$[5e] (285 mg) and [(dme)$NiBr_2$]. Yield 425 mg (0.87 mmol, 87%) as a blue, microcrystalline solid. Recrystallization from CH_2Cl_2/Et_2O afforded blue and red-brown crystals, but only the former were suitable for X-ray structure analysis. UV/Vis (CH_2Cl_2): λ (ε) = 550 nm (180 $M^{-1}\cdot cm^{-1}$), 600 (230), 1004 (90). NMR: no NMR signals due to paramagnetism. For crystallographic data see Tables 7 and 8; for further analytical data see Tables 11, 13, and 15.

General Procedure for the Synthesis of 9a, 9b, and 12: A solution of the respective *tripod* ligand **5** or **6** (0.5 mmol) in ethanol (15 mL) was added rapidly to a suspension of [(η^4-cod)$PdCl_2$] (145 mg, 0.5 mmol) in ethanol (10 mL). Within a few minutes the yellow reaction mixture was clearing up. After stirring at 25°C for 12 h, all volatiles were removed in vacuo. The residual solid was washed with portions of diethyl ether (10 mL, 3×) and dried in vacuo. **9a**: Starting material **5a** (270 mg). Yield 265 mg (0.37 mmol, 74%) as a colourless, microcrystalline solid. Recrystallization from CH_2Cl_2/Et_2O afforded colourless crystals suitable for X-ray structure analysis. ^{31}P NMR (CD_2Cl_2): δ = 15.8 (s, PPh_2) ppm. ^{31}P NMR (CD_2Cl_2, −100°C): δ = 15.8 (d, $^2J_{PP}$ = 115 Hz, PPh_2), 15.9 (d, $^2J_{PP}$ = 115 Hz, PPh_2) ppm. **9b**: Starting material **5b** (280 mg). Yield 255 mg (0.34 mmol, 69%) as a pale yellow microcrystalline solid. ^{31}P NMR (CD_2Cl_2): δ = 15.8 [br. s, PPh_2, $P(m\text{-Tol})_2$] ppm. ^{31}P NMR (CD_2Cl_2, −100°C): δ = 14.9−15.8 (m), 16.6−17.1 (m) ppm. **12**: Starting material **6a** (210 mg). Yield 245 mg (0.41 mmol, 82%) as a yellow, microcrystalline solid. Recrystallization from CH_2Cl_2/Et_2O afforded yellow crystals suitable for X-ray structure analysis. ^{31}P NMR (CD_2Cl_2): δ = 9.8 (s, PPh_2) ppm. For crystallographic data see Tables 7 and 8; for further analytical data see Tables 11, 13, and 15.

Synthesis of 10: A solution of the *tripod* ligand **5a** (135 mg, 0.25 mmol) in ethanol/THF (2:1; 15 mL) was added rapidly to a suspension of [*cis*-$(CH_3CN)_2PtCl_2$] (85 mg, 0.25 mmol) in ethanol (10 mL). Within a few minutes the reaction mixture was clearing up and the platinum complex precipitated. After stirring at 25°C for 12 h, all volatiles were removed in vacuo. The residual solid was washed with portions of diethyl ether (10 mL, 3×) and dried in vacuo. Recrystallization from CH_2Cl_2/Et_2O afforded 150 mg (0.19 mmol, 75%) of **10** as colourless crystals. ^{31}P NMR (CD_2Cl_2): δ = −2.5 (s, with Pt satellites, $^1J_{PtP}$ = 1720 Hz, PPh_2). ^{31}P NMR (CD_2Cl_2, −100°C): δ = −3.2 (d, $^2J_{PP}$ = 20 Hz, PPh_2), −2.5 (d, $^2J_{PP}$ = 20 Hz, PPh_2). For further analytical data, see Tables 11, 13, and 15.

Synthesis of 16a·PF_6: Solid $TlPF_6$ (2 equiv., 210 mg) was added, at 0°C, to a suspension of **7a** (200 mg, 0.3 mmol) in THF (50 mL) to

Table 13. Chemical shifts (δ values) and coupling constants J in the $^{13}C\{^1H\}$ NMR spectra of **7**−**18** in CH_2Cl_2

Compd.[a][b]	CH_2N	CH_2O	CH_2P	OCH_3	C_q	Pyrazole-C C4[c]	C5[c]	C3[c]	Aryl-C	Others
7a	58.5	72.7	29.1	57.7	42.3	105.8 br. s	133.2 br. s	140.2 br. s	129.0−136.3 m	
7b	58.3	72.7	28.7 m	57.6	42.3	105.6	132.6	140.0	128.8−140.2 m	21.7, 21.8 *m*-CH_3
7d	58.0	73.1	30.3	57.6	43.4	–	–	–	128.8−138.8 m	108.9, 122.6 pyrrole-*C*
8	57.4	72.6	26.4	57.7	42.6	105.5	131.5	139.8	128.7−139.8 m	
9a	59.8 t $^3J_{CP}$ = 11.0	72.3 t $^3J_{CP}$ = 5.2	30.7−31.5 m	57.4	43.9	105.8	131.7	140.1	128.8−136.2 m	
9b	59.6 t $^3J_{CP}$ = 11.0	72.3 br. s	30.7−31.4 m	57.5	43.8	105.8	131.6	140.0	128.8−138.9 m	21.6, 21.7 *m*-CH_3
10	59.9 $^3J_{CP}$ = 11.6	72.1 t $^3J_{CP}$ = 5.1	29.9−30.8 m	57.5	43.9	105.8	131.7	140.1	128.8−136.1 m	
12	52.4 br. s[d], 54.0 br. s[e]	68.6 br. s	29.4 d $^1J_{CP}$ = 27.7	58.2	45.2	105.9[e], 108.5[d]	131.8[e], 136.2[d]	140.3[e], 145.5[d]	128.8−132.7 m	
16a·PF$_6$	60.3 br. s	74.0 br. s	30.6-31.3 m	57.5	43.6	105.9	132.2	140.2	129.8−134.5 m	72.6 allyl-CH_2, 117.6 allyl-*C*H
17	59.0 dd $^3J_{CP}$ = 6.0, 10.5	74.6 dd $^3J_{CP}$ = 5.5, 7.4	27.8 dd, 29.9 dd $^1J_{CP}$ = 18.0, $^3J_{CP}$ = 8.8	58.0	42.5 br. s	105.6	131.4	139.6	127.2−140.3 m	20.0 *p*-CH_3 26.8 *o*-CH_3
18	60.8 t $^3J_{CP}$ = 10.6	72.8 t $^3J_{CP}$ = 5.9	32.2 dd, 34.5 dd $^1J_{CP}$ = 27.6, $^3J_{CP}$ = 9.8	57.3	44.2 br. s	105.8	131.6	139.7	128.6−140.1 m	14.5 dd Pd-CH_3 $^2J_{CP}$ = 6.0, 103.0

[a] All signals are singlets unless otherwise stated; d = doublet; dd = doublet of doublet; t = triplet; m = multiplet; (o) = overlapped. [b] Coupling constants in Hz. [c] See Scheme 13 for numbering scheme of the pyrazole. [d] Coordinated CH_2pz group. [e] Noncoordinated CH_2pz group.

Table 14. Analytical data of ligands **2**−**6**

Compd.	Formula	M [g/mol]	EI-MS [m/z (%)]	$C_{calcd.}/C_{found}$	$H_{calcd.}/H_{found}$	$N_{calcd.}/N_{found}$	$P_{calcd.}/P_{found}$
2b	$C_{21}H_{22}NOP$	335.38	336 (100), 305 (39), 199 (57), 183 (66), 120 (97)	75.21/75.33	6.61/6.95	4.18/3.61	9.24/n. d.
3b	$C_{34}H_{36}N_2OP_2$	550.62	551 (28), 474 (100), 460 (76)	74.17/74.25	6.59/6.88	5.09/4.89	11.25/n. d.
3c	$C_{38}H_{44}N_2OP_2$	606.73	607 (15), 529 (5), 487 (100),369 (10), 337 (11)	75.23/75.46	7.31/7.98	4.62/4.40	10.21/n. d.
3d	$C_{32}H_{44}N_2OP_2$	534.66	534 (1), 452 (100), 183 (10)	71.89/71.67	8.29/8.15	5.24/5.10	11.59/11.47
3e	$C_{33}H_{33}NOP_2$	521.57	521 (10), 444 (100), 199 (14), 183 (24)	75.99/75.98	6.38/6.63	2.69/2.49	11.88/n. d.
4b	$C_{29}H_{37}N_4OP$	488.61	489 (49), 473 (67), 407 (22), 369 (45), 269 (100), 250 (39)	71.29/72.00	7.63/8.43	11.47/10.74	6.34/n. d.
5a	$C_{33}H_{34}N_2OP_2$	536.59	536 (11), 459 (100), 183 (10)	73.87/73.98	6.39/6.39	5.22/5.26	11.54/11.71
5b	$C_{35}H_{38}N_2OP_2$	564.64	564 (18), 487 (100), 473 (77), 183 (14)	74.45/74.71	6.78/7.07	4.96/4.84	10.97/n. d.
5c	$C_{39}H_{46}N_2OP_2$	620.75	620 (2), 543 (2), 501 (100), 269 (10)	75.46/75.50	7.47/7.65	4.51/4.49	9.98/n. d.
5d	$C_{34}H_{35}NOP_2$	535.60	535 (8), 458 (100), 199 (10), 183 (13)	76.24/76.11	6.59/6.58	2.62/2.54	11.57/11.50
6a	$C_{24}H_{27}N_4OP$	418.47	418 (100), 341 (82), 337 (52), 305 (37), 269 (59), 199 (52), 183 (44), 151 (36)	68.88/69.19	6.50/6.68	13.39/12.77	7.40/n. d.
6b	$C_{30}H_{39}N_4OP$	502.64	502 (100), 487 (41), 421 (34), 383 (59)	71.69/71.74	7.82/8.06	11.15/11.02	6.16/6.18

yield a white precipitate of TlCl. After stirring the reaction mixture at 0°C for 1 h, allylmagnesium bromide (0.35 mL of a 1 M solution in THF) was added dropwise. After stirring at 25°C for 10 h, the precipitate was filtered off through 2 cm of Kieselguhr and all volatiles were removed in vacuo. The orange-coloured residue was washed with portions of diethyl ether (10 mL, 2×) and then recrystallized from CH_2Cl_2/Et_2O to give 170 mg (0.22 mmol, 72%) of **16a·PF$_6$**·0.75CH_2Cl_2 as air-stable, yellow crystals suitable for X-ray structure analysis. ^{31}P NMR (CD_2Cl_2): δ = −144.0 (sept, $^1J_{PF}$ = 712 Hz, PF_6^-), 13.0 (s, PPh_2) ppm. For crystallographic data see Table 9; for further analytical data see Tables 11, 13, and 15.

Synthesis of 16b·PF$_6$: A solution of the *tripod* ligand $EtOCH_2C(CH_2PPh_2)(CH_2pz)_2$[5e] (130 mg, 0.3 mmol) in EtOH (10 mL) was added rapidly to a suspension of $[Pd(\eta^3\text{-}C_3H_5)Cl]_2$ (55 mg, 0.15 mmol) in EtOH (10 mL). When a clear solution had formed (after about 30 min), solid KPF_6 (55 mg, 0.3 mmol) was added and within a few minutes the allyl complex precipitated. For complete precipitation the reaction mixture was cooled overnight to −30°C and afterwards filtered. The resultant grey residue was washed with portions of diethyl ether (10 mL, 2×), dried in vacuo, and recrystallized from CH_2Cl_2/Et_2O to give 140 mg (0.19 mmol, 64%) of **16b·PF$_6$** as air-stable, colourless crystals suitable for X-ray structure analysis. ^1H NMR and ^{13}C NMR: due to dynamic processes, no sharp signals could be detected. ^{31}P NMR (CD_2Cl_2): δ = −144.2 (sept, $^1J_{PF}$ = 710 Hz, PF_6^-), 11.5 (s, PPh_2) ppm. For crystallographic data see Table 9; for further analytical data see Tables 11, 13, and 15.

Synthesis of 17: A solution of the *tripod* ligand **5a** (270 mg, 0.5 mmol) in toluene (15 mL) was added to a solution of [*trans*-$(PPh_3)_2Ni(Mes)Br$] (390 mg, 0.5 mmol) in toluene (15 mL). After stirring the orange-coloured reaction mixture at 25°C for 10 h, the solvent was removed in vacuo. The crude product was suspended in petroleum ether (20 mL). After filtration of the suspension, the residue was washed carefully with portions of petroleum ether

Table 15. Analytical data of metal complexes **7**−**19**

Compd.	Formula	*M* [g/mol]	FAB-MS [*m/z* (%)]	$C_{calcd.}/C_{found}$	$H_{calcd.}/H_{found}$	$N_{calcd.}/N_{found}$	$P_{calcd.}/P_{found}$	$Cl_{calcd.}/Cl_{found}$
7a	$C_{33}H_{34}Cl_2N_2NiOP_2$	666.18	664 (4), 629 (100), 594 (18), 459 (36), 409 (24), 364 (31), 351 (28)	59.50/59.14	5.14/5.34	4.21/4.07	9.30/8.94	10.64/10.73
7b	$C_{35}H_{38}Cl_2N_2NiOP_2$	694.24	692 (4), 657 (100), 622 (10), 487 (19), 473 (16)	60.55/60.28	5.52/5.58	4.04/3.90	8.92/8.86	10.21/10.19
7c	$C_{39}H_{46}Cl_2N_2NiOP_2$	750.35	713 (50), 677 (100), 502 (59), 409 (85), 351 (42)	62.43/62.39	6.18/6.50	3.73/3.56	8.26/n. d.	9.45/n. d.
7d	$C_{34}H_{35}Cl_2NNiOP_2$	665.19	663 (4), 628 (100), 593 (18), 515 (35), 458 (34), 408 (15)	61.39/60.95	5.30/5.32	2.11/2.15	9.31/n. d.	10.66/n. d.
8	$C_{33}H_{34}Br_2N_2NiOP_2$	755.09	672 (69), 629 (54), 594 (17), 459 (25), 409 (15), 364 (18), 351 (15)	52.49/51.33	4.54/4.56	3.71/3.44	8.20/n. d.	21.16[a] /n. d.
9a	$C_{33}H_{34}Cl_2N_2OP_2Pd$	713.92	677 (100), 642 (17), 459 (77), 457 (50), 351 (59)	55.52/54.58	4.80/4.93	3.92/3.79	8.68/8.53	9.93/10.00
9b	$C_{35}H_{38}Cl_2N_2OP_2Pd$	741.97	705 (100), 670 (14), 487 (17)	56.66/56.32	5.16/5.13	3.78/3.64	8.35/8.44	9.56/9.52
10	$C_{33}H_{34}Cl_2N_2OP_2Pt$	802.58	801 (6), 766 (100), 731 (11), 634 (11), 459 (12)	49.39/49.50	4.27/4.55	3.49/3.35	7.72/7.35	8.83/9.20
11a	$C_{24}H_{27}Br_2N_4NiOP$	636.97	555 (28), 476 (100), 341 (10), 291 (28), 246 (64), 185 (38)	45.25/45.16	4.27/4.33	8.80/8.68	4.86/4.89	25.09[a]/24.85[b]
11b	$C_{24}H_{27}Cl_2N_4NiOP$	548.07	511 (88), 476 (76), 341 (26), 291 (49), 246 (100), 185 (47)	52.59/52.63	4.97/4.96	10.22/10.19	5.65/5.67	12.94/13.05
11c	$C_{25}H_{29}Br_2N_4NiOP$	651.00	569 (36), 490 (10), 431 (10), 355 (13), 327 (22), 305 (28), 281 (31), 246 (100)	46.12/45.56	4.49/4.55	8.61/8.44	4.76/4.72	24.55[a]/25.70[b]
12	$C_{24}H_{27}Cl_2N_4OPPd$	595.80	559 (100), 524 (28), 339 (81)	48.38/47.99	4.57/4.61	9.40/9.17	5.20/n. d.	11.90/n. d.
13	$C_{30}H_{39}Cl_2N_4NiOP$	632.23	595 (100), 559 (58), 502 (40), 488 (26), 435 (23), 383 (46)	56.99/56.88	6.22/6.27	8.86/8.94	4.90/4.89	11.22/11.21
14	$C_{14}H_{18}Br_2N_6Ni$	488.84	407 (100), 328 (29)	34.40/34.36	3.71/3.73	17.19/16.97		32.69[a]/32.43[b]
16a·PF$_6$	$C_{36}H_{39}F_6N_2NiOP_3$	781.32	635 (100), 594 (14), 409 (15), 364 (10)	52.24[c]/52.39	4.83[c]/4.88	3.32[c]/3.18	11.00[c]/n. d.	–
16b·PF$_6$	$C_{28}H_{34}F_6N_4OP_2Pd$	724.96	578 (100), 422 (35), 353 (30)	46.39/46.08	4.73/4.48	7.73/7.73	8.54/n. d.	–
17	$C_{42}H_{45}BrN_2NiOP_2$	794.37	792 (1), 673 (14), 594 (100), 409 (35), 364 (44)	63.50/63.32	5.71/5.73	3.53/3.52	7.80/7.67	10.06[a]/n. d.
18	$C_{34}H_{37}ClN_2OP_2Pd$	693.50	692 (3), 677 (93), 657 (41), 642 (15), 565 (10), 457 (100), 351 (39)	58.89/58.60	5.38/5.60	4.04/3.99	8.93/8.54	5.11/5.10
19·PF$_6$	$C_{51}H_{53}F_6N_4NiOP_3$	1003.60	857 (32), 595 (98), 476 (100), 381 (42)	59.69[d]/58.53	5.24[d]/5.25	5.42[d]/5.51	8.99[d]/n. d.	–

[a] $Br_{calcd.}$. [b] Br_{found}. [c] Calculated for **16a·PF$_6$**·0.75CH_2Cl_2. [d] Calculated for **19·PF$_6$**·0.35CH_2Cl_2.

(10 mL, 3×) to remove PPh_3, and dried in vacuo to give 285 mg (0.36 mmol, 72%) of **17** as a yellow, microcrystalline solid. ^{31}P NMR (CD_2Cl_2): δ = −8.0 (d, $^2J_{PP}$ = 41 Hz, *P*Ph_2 *trans* to Mes^-), 23.2 (d, $^2J_{PP}$ = 41 Hz, *P*Ph_2 *trans* to Br^-) ppm. For further analytical data see Tables 11, 13, and 15.

Synthesis of 18: A solution of the *tripod* ligand **5a** (270 mg, 0.5 mmol) in CH_2Cl_2 (15 mL) was added to a solution of [(η^4-cod)PdMeCl] (135 mg, 0.5 mmol) in CH_2Cl_2 (15 mL). After stirring the colourless reaction mixture at 25°C for 10 h, the solvent was removed in vacuo. The crude product was suspended in petroleum ether (20 mL). After filtration of the suspension, the resultant grey residue was washed with portions of petroleum ether (15 mL, 3×) and dried in vacuo. Recrystallization from CH_2Cl_2/Et_2O afforded 295 mg (0.43 mmol, 85%) of **18** as colourless crystals suitable for X-ray structure analysis. ^{31}P NMR (CD_2Cl_2): δ = −6.3 (d, $^2J_{PP}$ = 48 Hz, *P*Ph_2 *trans* to Me^-), 25.7 (d, $^2J_{PP}$ = 48 Hz, *P*Ph_2 *trans* to Cl^-) ppm. For crystallographic data see Table 9; for further analytical data see Tables 11, 13, and 15.

Synthesis of 19·PF$_6$: A solution of the *tripod* ligand **6a** (210 mg, 0.5 mmol) in toluene (15 mL) was added to a solution of [*trans*-$(PPh_3)_2$Ni(Mes)Br] (390 mg, 0.5 mmol) in toluene (15 mL). After stirring the orange-coloured reaction mixture at 25°C for 10 h, the solvent was removed in vacuo and the solid residue was dissolved in THF (30 mL). Solid $TlPF_6$ (175 mg, 0.5 mmol) was added and a precipitate of TlBr appeared immediately. The reaction mixture was stirred at 25°C for 3 h and then filtered through 2 cm of Kieselguhr to remove the $TlPF_6$. The solvent was removed in vacuo and the crude product was suspended in petroleum ether (20 mL). After filtration of the suspension, the residue was washed carefully with portions of petroleum ether (15 mL, 3×) to remove PPh_3, and dried in vacuo. Recrystallization from CH_2Cl_2/Et_2O afforded 250 mg (0.25 mmol, 50%) of **19·PF$_6$** as yellow crystals suitable for X-ray structure analysis. ^1H NMR and ^{13}C NMR: due to dynamic processes, no sharp signals could be detected. ^{31}P NMR (CD_2Cl_2): δ = −144.0 (sept, $^1J_{PF}$ = 712 Hz, *P*F_6^-), −5.8 (d, $^2J_{PP}$ = 272 Hz, *P*Ph_3), 7.9 (d, $^2J_{PP}$ = 280 Hz, *P*Ph_3), 19.4 (d, $^2J_{PP}$ = 280 Hz, *P*Ph_2), 21.7 (d, $^2J_{PP}$ = 272 Hz, *P*Ph_2) ppm. For this compound a ^{31}P NMR pattern of two doublets corresponding to the two P donors is expected. Instead, two such patterns are observed (δ = −5.8/21.7 and 7.9/19.4 ppm). The large coupling constants are in accord with a *trans* position of the two P donors in each case. There are obviously two isomers, and only the structure of the one characterized by X-ray crystallography is known. Attempts to isolate the other isomer have, so far, failed. For crystallographic data see Table 9; for further analytical data see Tables 11, 13, and 15.

Acknowledgments

We are indebted to the Deutsche Forschungsgemeinschaft and the Fonds der Chemischen Industrie for financial support. One of us

(R. F.) is indebted to the local Graduiertenkolleg "Selektivität in der organischen und metallorganischen Synthese und Katalyse" for a scholarship. The technical support of T. Jannack (mass spectrometry) and the Microanalytical Laboratory of the Institute of Organic Chemistry is gratefully acknowledged.

[1] Phosphorus donors: [1a] H. Heidel, G. Huttner, G. Helmchen, *Z. Naturforsch., Teil B* **1993**, *48*, 1681. [1b] T. Seitz, A. Muth, G. Huttner, *Chem. Ber.* **1994**, *127*, 1837. [1c] T. Seitz, A. Muth, G. Huttner, *Z. Naturforsch., Teil B* **1995**, *50*, 1045. [1d] H. Heidel, G. Huttner, L. Zsolnai, *Z. Naturforsch., Teil B* **1995**, *50*, 729.

[2] Oxygen donors: [2a] J. Dale, S. B. Fredriksen, *Acta Chem. Scand.* **1992**, *46*, 271. [2b] T.-Y. Hsieh, M.-C. Cheng, S.-M. Peng, S.-T. Liu, *J. Chem. Soc., Dalton Trans.* **1994**, 3499. [2c] A. Muth, G. Reinhard, G. Huttner, T. Seitz, T. Klein, L. Zsolnai, *Z. Naturforsch., Teil B* **1994**, *49*, 889.

[3] Sulfur donors: [3a] S.-T. Liu, H.-E. Wang, M.-C. Cheng, S.-M. Peng, *J. Organomet. Chem.* **1989**, *376*, 333. [3b] S.-T. Liu, C.-H. Yieh, H.-J. Lu, *Phosphorus, Sulfur Silicon* **1989**, *44*, 261. [3c] S.-T. Liu, C.-L. Tsao, M. C. Cheng, S. M. Peng, *Polyhedron* **1990**, *21*, 2579. [3d] S.-T. Liu, K.-J. Liu, *Inorg. Chem.* **1990**, *29*, 4576. [3e] S.-C. Tsai, H.-E. Wang, C.-T. Huang, L.-M. Yiin, S.-T. Liu, *Chem. Ber.* **1995**, *128*, 151. [3f] G. Reinhard, R. Soltek, G. Huttner, A. Barth, O. Walter, L. Zsolnai, *Chem. Ber.* **1996**, *129*, 97. [3g] R. Soltek, G. Huttner, *Eur. J. Inorg. Chem.* **1998**, 1417. [3h] R. Soltek, G. Huttner, L. Zsolnai, A. Driess, *Inorg. Chim. Acta* **1998**, *269*, 143. [3i] P. Schober, R. Soltek, G. Huttner, L. Zsolnai, K. Heinze, *Eur. J. Inorg. Chem.* **1998**, 1407.

[4] Cp donors: [4a] B. Antelmann, U. Winterhalter, G. Huttner, B. C. Janssen, J. Vogelgesang, *J. Organomet. Chem.* **1997**, *545–546*, 407. [4b] B. Antelmann, G. Huttner, U. Winterhalter, *J. Organomet. Chem.* **1998**, *553*, 433. [4c] J. Vogelgesang, G. Huttner, E. Kaifer, P. Kircher, P. Rutsch, S. Cunskis, *Eur. J. Inorg. Chem.* **1999**, 2187. [4d] J. Vogelgesang, A. Frick, G. Huttner, P. Kircher, *Eur. J. Inorg. Chem.* **2001**, 949.

[5] Nitrogen donors: [5a] S.-T. Liu, C.-Y. Liu, *J. Org. Chem.* **1992**, *57*, 6079. [5b] H.-E. Wang, C.-Y. Liu, M.-C. Cheng, S.-M. Peng, S.-T. Liu, *Phosphorus, Sulfur Silicon* **1992**, *69*, 201. [5c] S.-T. Liu, C.-H. Yieh, H.-P. Dai, *Proc. Natl. Sci. Counc.* **1995**, *19*, 1. [5d] A. Jacobi, G. Huttner, U. Winterhalter, *Chem. Ber./Recueil* **1997**, *130*, 1279. [5e] A. Jacobi, G. Huttner, U. Winterhalter, S. Cunskis, *Eur. J. Inorg. Chem.* **1998**, 675. [5f] R. Faissner, G. Huttner, E. Kaifer, P. Rutsch, *Eur. J. Inorg. Chem.* **2003**, 1681–1693.

[6] A. Jacobi, G. Huttner, U. Winterhalter, *J. Organomet. Chem.* **1998**, *571*, 231.

[7] J. Karas, G. Huttner, K. Heinze, P. Rutsch, L. Zsolnai, *Eur. J. Inorg. Chem.* **1999**, 405.

[8] [8a] T. Seitz, G. Huttner, M. Büchner, *Z. Naturforsch., Teil B* **1994**, *49*, 1813. [8b] T. Seitz, A. Muth, G. Huttner, T. Klein, O. Walter, M. Fritz, L. Zsolnai, *J. Organomet. Chem.* **1994**, *469*, 155.

[9] V. Schulz, A. Frick, G. Huttner, *Eur. J. Inorg. Chem.* **2002**, 3111.

[10] A. Frick, V. Schulz, G. Huttner, *Eur. J. Inorg. Chem.* **2002**, 3129.

[11] A. W. Addison, T. N. Rao, J. Reedijk, J. van Rijn, G. C. Verschoor, *J. Chem. Soc., Dalton Trans.* **1984**, 1349.

[12] [12a] G. R. van Hecke, W. DeW. Horrocks Jr., *Inorg. Chem.* **1966**, *5*, 1968. [12b] L. H. Pignolet, W. DeW. Horrocks Jr., R. H. Holm, *J. Am. Chem. Soc.* **1970**, *92*, 1855. [12c] G. N. La Mar, E. O. Sherman, *J. Am. Chem. Soc.* **1970**, *92*, 2691.

[13] [13a] G. Binsch, H. Kessler, *Angew. Chem.* **1980**, *92*, 445; *Angew. Chem. Int. Ed. Engl.* **1980**, *19*, 411. [13b] K. Il'yasov, O. Nedopekin, *WIN-DYNAMICS 1.0 Release 951220, NMR Dynamic Spectra Simulation and Iteration*, Bruker-Franzen Analytik GmbH, Bremen, Germany (http://www.bruker.de).

[14] *Organikum*, Deutscher Verlag der Wissenschaften, Berlin, **1990**.

[15] P. Fresenius, K. Görlitzer, in: *Organisch-chemische Nomenklatur*, Wissenschaftliche Verlagsgesellschaft, Stuttgart, **1998**.

[16] *DENZO-SMN, Data Processing Software*, Nonius **1998** (http://www.nonius.com).

[17] [17a] G. M. Sheldrick, *SHELXS-97, Program for Crystal Structure Solution*, University of Göttingen, **1997**. [17b] G. M. Sheldrick, *SHELXL-97, Program for Crystal Structure Refinement*, University of Göttingen, **1997** (http://shelx.uni-ac.gwdg.de/shelx/index.html). [17c] *International Tables for X-ray Crystallography*, Kynoch Press, Birmingham, U.K., **1974**, vol. 4.

[18] L. Zsolnai, G. Huttner, *XPMA*, University of Heidelberg, **1994** (http://www.rzuser.uni-heidelberg.de/~il1/laszlo/xpm.html).

[19] R. Soltek, G. Huttner, *WinRay-32*, University of Heidelberg, **1998** (http://www.uni-heidelberg.de/institute/fak12/AC/huttner/html/winray.html).

[20] [20a] R. E. Ireland, D. M. Walba, *Org. Synth. Coll. Vol.* **1988**, *6*, 567. [20b] K. Issleib, H. O. Fröhlich, *Z. Naturforsch., Teil B* **1959**, *14*, 349.

[21] J. B. Lambert, J. H. So, *J. Org. Chem.* **1991**, *56*, 5960.

[22] R. M. Ceder, J. Cubillo, G. Muller, M. Rocamora, *J. Organomet. Chem.* **1992**, *429*, 391.

[23] R. E. Rülke, J. E. Ernsting, A. L. Spek, C. J. Elsevier, P. W. N. M. van Leeuwen, K. Vrieze, *Inorg. Chem.* **1993**, *32*, 5769.

Received September 23, 2002

